SIAM J. Imaging Sciences
Vol. 8, No. 2, pp. 939–967

Multifrequency Impedance Imaging with Multiple Signal Classification*

Roland Griesmaier† and Martin Hanke‡

Abstract. We consider a multifrequency impedance imaging technique that has recently been suggested as a modality for mammography screenings. This approach uses observations of boundary voltages generated by a collection of AC boundary currents that have the same spatial distribution and only differ in their driving frequency. The aim is to identify and determine the locations of small focal lesions. We analyze the potential and the limitations of a multiple signal classification-type reconstruction method for this setting. We prove that with sufficiently many different driving frequencies the position of a single planar obstacle will always be detected, but the identification of multiple obstacles may fail for certain exceptional geometrical configurations. We propose a modification of the original scheme for which the set of false negative configurations is reduced. It is also shown that, generically, the given measurements allow the determination of the conductivities and permittivities of the lesions to facilitate their classification. Finally, we provide arguments to support the claim that it should also be possible to extract shape information from these data. Our analysis is based on a well-known asymptotic expansion of solutions to the conductivity equation for infinitesimal planar obstacles and a novel description of the associated polarization tensors as meromorphic functions of frequency.

Key words. electrical impedance tomography, multiple frequencies, MUSIC, polarization tensor

AMS subject classifications. 35R30, 65N21

DOI. 10.1137/140992436

1. Introduction.

Some years ago Devaney [7] suggested the use of the MUltiple SIgnal Classification (MUSIC) algorithm from signal processing (cf., e.g., Therrien [18]) as a means for detecting small perturbations or obstacles from scattering measurements (see also his treatment of this topic in the recent book [8] or, e.g., [2, 6, 13]). His idea can easily be adapted to the (quasi-stationary) conductivity equation, and a rigorous justification of the method for this particular application has been provided in [3]. The basic assumption of this analysis is that voltage measurements generated by sufficiently many linearly independent spatially distributed boundary currents are available.

When this is not the case for whatever practical reasons one may alternatively consider to leave the quasi-stationary regime and apply AC currents of different, somewhat larger, frequencies to generate linearly independent boundary excitations. For example, this was suggested by Scholz [16] for the so-called TransScan TS2000, a commercial device for mammography screenings that only generates a single spatial boundary current distribution, but

*Received by the editors October 21, 2014; accepted for publication (in revised form) February 10, 2015; published electronically April 21, 2015.
http://www.siam.org/journals/siims/8-2/99243.html
†Institut für Mathematik, Universität Würzburg, 97074 Würzburg, Germany (roland.griesmaier@uni-wuerzburg.de).
‡Institut für Mathematik, Johannes Gutenberg-Universität Mainz, 55099 Mainz, Germany (hanke@math.uni-mainz.de).

can operate at various frequencies up to the kHz regime. In a very similar mathematical framework Ammari, Boulier, and Garnier [1] have recently suggested a model to explain the physical mechanisms that allow weakly electric fish to navigate in turbid water. In both works numerical experiments indicate that the MUSIC scheme can utilize appropriate AC data to locate small inhomogeneities, that is, focal lesions in the breast and obstacles in the neighborhood of the fish, respectively.

So far, there is no comprehensive theoretical justification of the MUSIC algorithm when applied to such multifrequency AC data, although Ammari, Boulier, and Garnier provide some preliminary explanations why the scheme may work well to detect a single small disk-shaped obstacle. In this paper we will elaborate on these results and prove that in two space dimensions the method works reliably for single small obstacles of arbitrary shape; moreover, we show that generically the given data not only allow us to determine the location of the obstacle but also its material properties, i.e., conductivity and permittivity, and we indicate ways to approximate these parameters. We also provide arguments suggesting that the acquired information is rich enough to retrieve information on the obstacle's shape as well. Last, but not least, we recommend and analyze a slight modification of the original algorithm—the *multifrequency MUSIC* scheme—for the reconstruction and identification of multiple obstacles.

The paper is organized as follows. In the next section we introduce the geometrical setup of our problem, which is similar to the one from [3]; alternative settings, such as those considered in [1] and [16] can be treated in much the same way. In this section we also review the frequency dependence of so-called polarization tensors, a key ingredient of our analysis below. The basic MUSIC variant from [1] is introduced in section 3, and in section 4 it is established that the method will always determine the location of a single small obstacle, provided that infinitely many probing frequencies are being used. Means to approximate material parameters and the shape of the obstacle are investigated in section 5.

From section 6 onwards we focus on the behavior of the MUSIC algorithm in the presence of two obstacles, and we start by exemplifying the superiority of a new multifrequency MUSIC scheme for this purpose. Then we derive a list—as complete as we possibly can—of all geometric constellations for which the multifrequency MUSIC scheme will fail to identify the obstacles: We begin with obstacles of different material parameters in section 7 and continue in section 8 with obstacles with identical material parameters. Finally, in section 9 we briefly comment on the case where only one of the two obstacles can be detected. We note that the results of sections 6–9 can also be used to understand the behavior of the MUSIC algorithm when more than two obstacles are present. Some numerical results to illustrate our findings are provided in section 10, and then we conclude with some final remarks.

2. Problem formulation.

Let $\mathcal{D} \subset \mathbb{R}^2$ be a bounded and simply connected domain with boundary $\partial\mathcal{D}$, and

$$\Omega = \bigcup_{l=1}^{l_*} \Omega_l \subset \mathcal{D}$$

a union of l_* separated obstacles Ω_l within $\mathcal{D}$. Imposing a (nontrivial) time-harmonic (AC) boundary current

$$F(x,t) = f(x)e^{\mathrm{i}\omega t}, \qquad x \in \partial\mathcal{D}, \ t \in \mathbb{R},$$

with driving frequency $\omega > 0$, where $f \in L^2(\partial\mathcal{D})$ has vanishing mean,

$$\int_{\partial\mathcal{D}} f \, \mathrm{d}s = 0 \,,$$

a time-harmonic potential

$$U(x,t) = u(x;\omega)e^{\mathrm{i}\omega t}$$

is generated in $\mathcal{D}$, and under suitable physical assumptions (cf., e.g., Cheney, Isaacson, and Newell [5]) its spatial component $u = u(\cdot;\omega)$ satisfies the boundary value problem

$$-\nabla\cdot(\gamma\nabla u) = 0 \quad \text{in } \mathcal{D}\,, \qquad \partial_\nu u = f \quad \text{on } \partial\mathcal{D}\,. \tag{2.1}$$

Here, the frequency dependent complex admittivity γ is assumed to be piecewise constant,

$$\gamma = \begin{cases} 1 & \text{in } \mathcal{D}\setminus\overline{\Omega}\,, \\ \sigma_l + \mathrm{i}\omega\varepsilon_l & \text{in } \Omega_l\,,\ l = 1,\dots,l_*\,, \end{cases}$$

where $\sigma_l > 0$ is the conductivity and $\varepsilon_l > 0$ the permittivity of the obstacle in Ω_l. This quasi-static approximation of Maxwell's equations represents a standard model for biomaterials that is valid within a certain frequency band (cf., e.g., Scholz and Anderson [17]); in the sequel it will be assumed without further notice that data are only being measured for corresponding frequencies.

Our aim is to determine the obstacles Ω_l from observations of boundary potentials

$$g = u|_\Gamma\,, \tag{2.2}$$

where Γ is a relatively open subset of $\partial\mathcal{D}$, and u is normalized to have vanishing mean on Γ. To this end we compare g with the reference potential

$$g_{\mathbb{1}} = u_{\mathbb{1}}|_\Gamma\,,$$

where $u_{\mathbb{1}}$ denotes the harmonic function given by

$$-\Delta u_{\mathbb{1}} = 0 \quad \text{in } \mathcal{D}\,, \qquad \partial_\nu u_{\mathbb{1}} = f \quad \text{on } \partial\mathcal{D}\,, \qquad \int_\Gamma u_{\mathbb{1}} \, \mathrm{d}s = 0\,,$$

that would be observed in the absence of any obstacles. We note that $u_{\mathbb{1}}$, and hence, $g_{\mathbb{1}}$ are independent of the driving frequency ω, whereas $g = g(\cdot;\omega)$ by virtue of (2.1)–(2.2). The differences $h = g - g_{\mathbb{1}}$ are the so-called *relative data* that we consider to be known on Γ. In this work the spatial distribution f of the boundary currents is fixed, but the driving frequency ω varies: We assume that we are given relative data $h_n \in L^2(\Gamma)$, $n = 1,2,\dots,n_*$, for $n_* \le \infty$ different frequencies ω_n, i.e.,

$$h_n(x) = g(x;\omega_n) - g_{\mathbb{1}}(x)\,, \qquad x \in \Gamma\,,\ n = 1,\dots,n_*\,. \tag{2.3}$$

We analyze the inverse problem in a restricted setting, assuming that the obstacles Ω_l are of small diameter, i.e., that

$$\Omega_l = x_l + \delta\mathcal{O}_l\,, \qquad l = 1,\dots,l_*\,, \tag{2.4}$$

where $x_l \in \mathcal{D}$, $l = 1, \dots, l_*$, are the pairwise different centers of mass of Ω_l, and the scaling parameter $\delta > 0$ is sufficiently close to zero. We refer to x_l and $\mathcal{O}_l$ as *position* and *shape* of the obstacle Ω_l, respectively, and note that—in contrast to the colloquial use of this term—the shape of an obstacle is not invariant under rotations and scalings. Throughout, the shapes of the obstacles are assumed to be simply connected with sufficiently smooth (e.g., C^2) boundaries. Under these assumptions it is well known that the relative data from (2.3) have the asymptotic expansion

$$h_n(x) = h_n^\delta(x) = \delta^2 \sum_{l=1}^{l_*} \nabla u_{\mathbb{1}}(x_l) \cdot M\big(\lambda^{(l)}(\omega_n); \mathcal{O}_l\big)\, \nabla_z N(x, x_l) + O(\delta^3)\,, \tag{2.5}$$

where the last term on the right-hand side is bounded by $C\delta^3$, uniformly for $x \in \Gamma$ and $1 \le n \le n_*$, (cf., e.g., Cedio-Fengya, Moskow, and Vogelius [4] or Ammari and Kang [2]; the uniformity w.r.t. x and n can be seen by combining the argument of [10, Thm. 4.1] with the one in [2, Lemma 2.18]). Here, $N(\cdot, z)$ is the Neumann function for the negative Laplacian in $\mathcal{D}$ with singularity in $z \in \mathcal{D}$, which satisfies

$$-\Delta N(\cdot, z) = \delta_z \quad \text{in } \mathcal{D}\,, \qquad \partial_\nu N(\cdot, z) = -\frac{1}{|\partial\mathcal{D}|} \quad \text{on } \partial\mathcal{D}\,, \qquad \int_\Gamma N(\cdot, z)\, \mathrm{d}s = 0\,,$$

and $\nabla_z N$ denotes its gradient with respect to the second argument. The complex symmetric 2×2 matrix $M(\lambda^{(l)}(\omega); \mathcal{O}_l)$ is the so-called *polarization tensor* (cf. [2]) associated with the shape $\mathcal{O}_l$ of the respective obstacle and its *admittivity contrast*

$$\lambda^{(l)}(\omega) = \frac{1}{2}\frac{1 + \sigma_l + \mathrm{i}\omega\varepsilon_l}{1 - \sigma_l - \mathrm{i}\omega\varepsilon_l}\,. \tag{2.6}$$

Under the given assumptions the polarization tensor is a meromorphic function of[1] $\lambda \in \widehat{\mathbb{C}} \setminus \{0\}$ of the form

$$M(\lambda; \mathcal{O}) = \begin{bmatrix} \displaystyle\sum_{k\in\mathbb{N}} \left(\frac{r_k^2}{\lambda - \lambda_k} + \frac{r_{-k}^2}{\lambda + \lambda_k}\right) & \displaystyle\sum_{k\in\mathbb{N}} c_k \left(\frac{r_k r_{-k}}{\lambda - \lambda_k} - \frac{r_k r_{-k}}{\lambda + \lambda_k}\right) \\ \displaystyle\sum_{k\in\mathbb{N}} c_k \left(\frac{r_k r_{-k}}{\lambda - \lambda_k} - \frac{r_k r_{-k}}{\lambda + \lambda_k}\right) & \displaystyle\sum_{k\in\mathbb{N}} \left(\frac{r_{-k}^2}{\lambda - \lambda_k} + \frac{r_k^2}{\lambda + \lambda_k}\right) \end{bmatrix} \tag{2.7}$$

(cf. [9]), where $|\lambda_k|$ runs through pairwise different nonnegative Fredholm eigenvalues of $\mathcal{O}$ (or $\partial\mathcal{O}$), $r_{\pm k} \in \mathbb{R}$ (not all of them being zero), and $0 \le c_k \le 1$ for each $k \in \mathbb{N}$; if some $\lambda_k = 0$ then we may assume without loss of generality r_{-k} to be 0 and c_k to be 1. Later we repeatedly refer to the (j,k)-entry of the matrix $M(\lambda; \mathcal{O})$ as $M_{jk}(\lambda; \mathcal{O})$. We recall (cf. Plemelj [15], or Khavinson, Putinar, and Shapiro [12]) that the Fredholm eigenvalues of $\mathcal{O}$ are the eigenvalues of the compact double layer integral operator over $\partial\mathcal{O}$. These eigenvalues belong to the interval $[-1/2, 1/2)$, and only cluster at $\lambda = 0$. The eigenvalue $-1/2$ is a trivial one (its eigenfunctions are the constant functions on $\partial\mathcal{O}$ when $\mathcal{O}$ is simply connected), and this one does not occur

[1] As usual, $\widehat{\mathbb{C}} = \mathbb{C} \cup \{\infty\}$.

in (2.7); being in two space dimensions, the other eigenvalues come in pairs $\pm\lambda_k$ symmetric to the origin.

Example 2.1. An important example of a shape that we will repeatedly refer to is the ellipse $\mathcal{O} = \mathcal{E}$ with half axes of length $\delta_{1,2} > 0$, the first of which being given by $\delta_1 Q_\theta e_1$, where

$$e_1 = \begin{bmatrix} 1 \\ 0 \end{bmatrix} \qquad \text{and} \qquad Q_\theta = \begin{bmatrix} \cos\theta & -\sin\theta \\ \sin\theta & \cos\theta \end{bmatrix} \tag{2.8}$$

with $\theta \in (-\pi/2, \pi/2]$. The corresponding polarization tensor is

$$M(\lambda;\mathcal{E}) = |\mathcal{E}| \begin{bmatrix} \dfrac{\cos^2\theta}{\lambda-\lambda_\mathcal{E}} + \dfrac{\sin^2\theta}{\lambda+\lambda_\mathcal{E}} & \dfrac{\sin\theta\,\cos\theta}{\lambda-\lambda_\mathcal{E}} - \dfrac{\sin\theta\,\cos\theta}{\lambda+\lambda_\mathcal{E}} \\ \dfrac{\sin\theta\,\cos\theta}{\lambda-\lambda_\mathcal{E}} - \dfrac{\sin\theta\,\cos\theta}{\lambda+\lambda_\mathcal{E}} & \dfrac{\sin^2\theta}{\lambda-\lambda_\mathcal{E}} + \dfrac{\cos^2\theta}{\lambda+\lambda_\mathcal{E}} \end{bmatrix}$$

with $|\mathcal{E}| = \pi\delta_1\delta_2$ denoting the area of $\mathcal{E}$ and

$$\lambda_\mathcal{E} = \frac{1}{2}\frac{\delta_2 - \delta_1}{\delta_2 + \delta_1}\,. \tag{2.9}$$

For this geometry the polarization tensor $M(\lambda;\mathcal{E})$ is a diagonal matrix, if and only if the two half axes of $\mathcal{E}$ are aligned with the coordinate axes.

The special case of a disk is included by setting $\delta_1 = \delta_2$, in which case

$$M(\lambda;\mathcal{E}) = \frac{|\mathcal{E}|}{\lambda}\, I$$

with a single pole at $\lambda_\mathcal{E} = 0$, only; here, I is the 2×2 identity matrix. ■

For later reference we list some further properties of the polarization tensor for a given shape $\mathcal{O}$. (See [2] for the first two properties, and [9] for the last one). First, the polarization tensor is positive definite when $\lambda > 1/2$ and negative definite when $\lambda < -1/2$. Second, if two shapes $\mathcal{O}_1$ and $\mathcal{O}_2$ are geometrically *similar*, i.e., there exists an orthogonal transformation $Q \in \mathbb{R}^{2\times 2}$ and a scaling factor $c > 0$, such that $\mathcal{O}_2 = cQ(\mathcal{O}_1)$ then there holds

$$M(\cdot;\mathcal{O}_2) = M\big(\cdot;cQ(\mathcal{O}_1)\big) = c^2 Q M(\cdot;\mathcal{O}_1) Q^*\,. \tag{2.10}$$

Finally, the polarization tensor as a function of λ provides substantial information about the shape of a domain. For example, if $\mathcal{O}_1$ is an ellipse and $\mathcal{O}_2$ has the same polarization tensor as $\mathcal{O}_1$ for all $\lambda \in \widehat{\mathbb{C}} \setminus [-1/2, 1/2)$ then $\mathcal{O}_2 = \mathcal{O}_1$.

Definition 2.2. *Two bounded simply connected planar shapes $\mathcal{O}_1$ and $\mathcal{O}_2$ are called* polarization equivalent *to each other, if the corresponding polarization tensors $M(\lambda;\mathcal{O}_1)$ and $M(\lambda;\mathcal{O}_2)$ are the same meromorphic functions of $\lambda \in \widehat{\mathbb{C}} \setminus \{0\}$.*

It follows immediately from the basic definition of polarization tensors that two polarization equivalent shapes must have the same volume (cf., e.g., [9]).

Example 2.3. As an example for two polarization equivalent shapes consider an arbitrary shape $\mathcal{O}_1$ and its rotation by π, i.e., $\mathcal{O}_2 = -\mathcal{O}_1$. By virtue of (2.10) $\mathcal{O}_1$ and $\mathcal{O}_2$ have the same polarization tensor, although the shapes are different in general. ■

We believe that two polarization equivalent shapes are, indeed, equal up to rotations by π, but so far this is an open problem.

3. The MUSIC scheme. On the grounds of the basic assumption that the obstacles Ω_l are of small diameter, parameterized by the value of $\delta > 0$ in (2.4), it follows from (2.5) that the rescaled leading order term h_n° of the relative data $h_n = h_n^\delta$ of (2.3) is a superposition of l_* complex dipoles located at the positions of the obstacles, i.e.,

$$\frac{1}{\delta^2}\, h_n^\delta \;\approx\; h_n^\circ = \sum_{l=1}^{l_*} p_l(\omega_n) \cdot \nabla_z N(\cdot, x_l)\,, \tag{3.1}$$

where the dipole moments

$$p_l(\omega_n) = M\big(\lambda^{(l)}(\omega_n); \mathcal{O}_l\big)\nabla u_{\mathbb{1}}(x_l) \;\in\; \mathbb{C}^2 \tag{3.2}$$

depend on the shapes and the material parameters of the obstacles, the driving frequency ω_n, and the gradient of the reference potential $u_{\mathbb{1}}$ at the obstacles' centers.

In the original MUSIC algorithm (cf. [3]) one selects an arbitrary vector $p \in \mathbb{R}^2 \setminus \{0\}$, and checks whether for a given test point $z \in \mathcal{D}$ the function

$$\phi_{z,p} \;:=\; p \cdot \nabla_z N(\cdot, z)\big|_\Gamma\,, \tag{3.3}$$

i.e., the trace on Γ of a dipole potential with dipole moment p located in the test point z exhibits a good match with the given data. For the analysis of the MUSIC scheme in [3] the choice of the dipole moment p had not been essential; concerning the AC variant of the method Ammari, Boulier, and Garnier [1] suggest choosing

$$p = p_z = \nabla u_{\mathbb{1}}(z)\,, \tag{3.4}$$

because this is—up to a scalar multiple—the exact dipole moment $p_l(\omega_n)$ in (3.2), if the obstacle Ω_l located in $x_l = z$ has the shape of a disk (cf. Example 2.1).

The pattern matching step of the algorithm is based on Proposition 3.1 below. To formulate this result we define $A_\delta : \ell^1(n_*) \to L^2(\Gamma)$ via

$$(A_\delta \boldsymbol{a})(x) = \sum_{n=1}^{n_*} a_n h_n^\delta(x)\,, \qquad x \in \Gamma\,,$$

where $\boldsymbol{a} \in \ell^1(n_*)$ is the complex-valued sequence

$$\boldsymbol{a} = [a_1, \ldots, a_{n_*}]^T\,.$$

By virtue of (3.1), $\delta^{-2} A_\delta \to A_\circ$ in $\mathscr{L}(\ell^1(n_*), L^2(\Gamma))$ as $\delta \to 0$, where

$$A_\circ \boldsymbol{a} = \sum_{n=1}^{n_*} a_n h_n^\circ = \sum_{l=1}^{l_*} \Big(\sum_{n=1}^{n_*} a_n p_l(\omega_n) \Big) \cdot \nabla_z N(\cdot, x_l)\big|_\Gamma \tag{3.5}$$

and $\mathscr{L}(\ell^1(n_*), L^2(\Gamma))$ denotes the space of bounded linear operators from $\ell^1(n_*)$ to $L^2(\Gamma)$. Concerning $A_\circ$ we have the following result.

Proposition 3.1. *Let $p \in \mathbb{C}^2 \setminus \{0\}$, $z \in \mathcal{D}$, and define $\phi_{z,p}$ as in (3.3).*

(a) *If $\phi_{z,p} \in \mathcal{R}(A_\circ)$ then there holds $z \in \{x_1, \ldots, x_{l_*}\}$.*

(b) *For a given $1 \le l \le l_*$ one has $\phi_{x_l,p} \in \mathcal{R}(A_\circ)$ if and only if the $2l_* \times n_*$ dimensional linear system*

$$0 = \sum_{n=1}^{n_*} a_n p_j(\omega_n)\,, \quad j \neq l\,, \qquad p = \sum_{n=1}^{n_*} a_n p_l(\omega_n)\,, \tag{3.6}$$

has a solution $\boldsymbol{a} = [a_1, \ldots, a_{n_*}]^T \in \ell^1(n_*)$.

Proof.

(a) For $z \in \mathcal{D}$, $p \in \mathbb{C}^2 \setminus \{0\}$, and $\boldsymbol{a} \in \ell^1(n_*)$ the potentials $w = p \cdot \nabla_z N(\cdot, z)$ and

$$v = \sum_{l=1}^{l_*} \left(\sum_{n=1}^{n_*} a_n p_l(\omega_n) \right) \cdot \nabla_z N(\cdot, x_l)$$

are harmonic functions in $\mathcal{D} \setminus \{z\}$ and $\mathcal{D} \setminus \{x_1, \ldots, x_{l_*}\}$, respectively, with homogeneous Neumann data on $\partial\mathcal{D}$. Accordingly, if $\phi_{z,p} = w|_\Gamma \in \mathcal{R}(A_\circ)$ then w and v—for suitably chosen a_n—are harmonic functions with the same Cauchy data on Γ and, hence, they coincide in $\mathcal{D} \setminus \{x_1, \ldots, x_{l_*}, z\}$. Moreover, as v is bounded at any $x \notin \{x_1, \ldots, x_{l_*}\}$ while w fails to be bounded near $x = z$, we necessarily have $z \in \{x_1, \ldots, x_{l_*}\}$ as has been claimed.

(b) Obviously, if (3.6) holds true for some $\boldsymbol{a} \in \ell^1(n_*)$ then $\phi_{x_l,p} = A_\circ \boldsymbol{a} \in \mathcal{R}(A_\circ)$. Now assume that $\phi_{x_l,p} \in \mathcal{R}(A_\circ)$ for some $p \in \mathbb{C}^2 \setminus \{0\}$. Then $\phi_{x_l,p} = A_\circ \boldsymbol{a}$ for some $\boldsymbol{a} \in \ell^1(n_*)$ and, hence,

$$p \cdot \nabla_z N(x, x_l) = \sum_{j=1}^{l_*} \left(\sum_{n=1}^{n_*} a_n p_j(\omega_n) \right) \cdot \nabla_z N(x, x_j)\,, \qquad x \in \Gamma\,.$$

As in the first part of the proof it follows that this identity extends to $x \in \mathcal{D} \setminus \{x_1, \ldots, x_{l_*}\}$, and since its left-hand side is bounded near all $x_j \neq x_l$, all dipole moments $\sum_{n=1}^{n_*} a_n p_j(\omega_n)$ with $j \neq l$ must vanish, while

$$\sum_{n=1}^{n_*} a_n p_l(\omega_n) = p$$

for $j = l$. This proves (3.6). ∎

Based on this result, and since $\mathcal{R}(A_\circ)$ is close to $\mathcal{R}(A_\delta)$ by virtue of (3.5), a test point $z \in \mathcal{D}$ is considered in [1] to be the (approximate) location of an obstacle if, with p_z the dipole moment of (3.4),

$$\phi_{z,p_z} \in \mathcal{R}(A_\delta) \tag{3.7}$$

in a suitable approximate sense, which resembles the usual pattern matching procedure of a principal component analysis. In fact, in practice, when n_* is a finite number, A_δ can be

considered an operator from $\mathbb{R}^{n_*}$ to $L^2(\Gamma)$, and generic elements from $\mathcal{R}(A_\circ)$ have a small distance to the span of the dominating left singular vectors of $A_\delta : \mathbb{R}^{n_*} \to L^2(\Gamma)$. It follows that the fraction of the norm of the component of ϕ_{z,p_z} within this span over the norm of its orthogonal complement gets large, when ϕ_{z,p_z} belongs to the range space of $A_\circ$, and is of moderate size otherwise. Thus, a color coded plot of the logarithm of this fraction provides a good visualization of the locations of the obstacles (see the numerical examples in section 10).

However, according to Proposition 3.1(b), the test (3.7) may fail in that z is the location of an obstacle, but ϕ_{z,p_z} does not belong to the range of $A_\circ$. So far, no conclusive analysis of this problem has been given in the literature; it is the purpose of this paper to clarify the circumstances under which such failures may occur. A trivial reason for a failure of this test is a vanishing gradient of $u_{\mathbb{1}}$ at the position of some obstacle. Such a trivial failure cannot be cured without sending in a different spatial current distribution f. On the other hand, for many boundary currents it can be excluded beforehand that $\nabla u_{\mathbb{1}}$ vanishes in $\mathcal{D}$ at all (cf., e.g., Isakov [11, section 4.4]).

In what follows we therefore assume throughout that $\nabla u_{\mathbb{1}}(x) \neq 0$ for all $x \in \mathcal{D}$.

4. Reconstruction of the position of a single obstacle. In this section we treat the case of a single planar obstacle, as was the main focus of the preliminary analysis in [1]. In this case it is obvious that the test (3.7) requires at least $n_* \geq 2$ test frequencies to allow for a realistic chance of achieving the second equation of (3.6). In our analysis, however, we will go much further, and assume that data have been generated for $n_* = \infty$ frequencies.

To begin with, we establish that under our assumptions the position x_1 of a single obstacle Ω_1 can always be reconstructed by the algorithm described above.

Theorem 4.1. *Assume that $\mathcal{D}$ contains a single obstacle Ω_1 of the form (2.4), and that $\nabla u_{\mathbb{1}}(x_1) \neq 0$. Moreover, let $\mathcal{R}(A_\circ)$ be the span of the limiting operator $A_\circ : \ell^1 \to L^2(\Gamma)$ from (3.5) for infinitely many probing frequencies $\omega_n \in (0,\infty)$, $n \in \mathbb{N}$. Then there holds $\phi_{z,p_z} \in \mathcal{R}(A_\circ)$ if and only if $z = x_1$.*

Proof. Recalling Proposition 3.1(a) we only have to prove that $\phi_{x_1,p_{x_1}} \in \mathcal{R}(A_\circ)$. To this end we choose the coordinate system in such a way that $p_{x_1} = \nabla u_{\mathbb{1}}(x_1)$ is pointing in the direction of the first standard basis vector e_1. Then we conclude from Proposition 3.1(b) and (3.2) that $\phi_{x_1,p_{x_1}} \in \mathcal{R}(A_\circ)$ if and only if there is a vector $\boldsymbol{a} = [a_n] \in \ell^1$ such that

$$e_1 = \sum_{n=1}^{\infty} a_n M\big(\lambda^{(1)}(\omega_n); \mathcal{O}_1\big) e_1 \,,$$

which is equivalent to saying that there is no scalar $c \in \mathbb{C}$ such that

$$M_{11}\big(\lambda^{(1)}(\omega_n); \mathcal{O}_1\big) = c M_{21}\big(\lambda^{(1)}(\omega_n); \mathcal{O}_1\big) \qquad \text{for all } n \in \mathbb{N} \tag{4.1}$$

(cf., e.g., Kress [14, Lemma 4.14]).

At this stage we recall that each component $M_{jk}(\lambda; \mathcal{O})$ of the polarization tensor is a meromorphic function of $\lambda \in \widehat{\mathbb{C}} \setminus \{0\}$. Moreover, $\lambda = \lambda^{(1)}(\omega)$ from (2.6) is a Möbius transformation of ω, with inverse transformation

$$\omega^{(1)}(\lambda) = \frac{1 - 2\lambda + (1+2\lambda)\sigma_1}{(1+2\lambda)\varepsilon_1}\,\mathrm{i}\,. \tag{4.2}$$

Accordingly, $M_{jk}(\lambda^{(1)}(\omega);\mathcal{O})$ is a meromorphic function of $\omega \in \widehat{\mathbb{C}}\setminus\{(1+\sigma_1)\mathrm{i}/\varepsilon_1\}$, and it follows from the uniqueness theorem for meromorphic functions in the extended complex plane that if (4.1) holds for infinitely many frequencies $\omega_n \in (0,\infty)$ then it holds everywhere, i.e.,

$$M_{11}(\cdot;\mathcal{O}_1) = cM_{21}(\cdot;\mathcal{O}_1)\,. \tag{4.3}$$

The latter, however, cannot be true, because $M_{21}(\lambda;\mathcal{O}_1)$ is an even function of $\lambda \in \mathbb{R}$ by virtue of (2.7), whereas $M_{11}(\lambda;\mathcal{O}_1)$ is a strictly decreasing function of $\lambda \in \mathbb{R}$ (except for its poles). It thus follows that neither (4.3) nor (4.1) can hold true for any value of $c \in \mathbb{C}$, which was to be shown. ∎

This proves that the MUSIC scheme with infinitely many probing frequencies will not fail in reconstructing the position of a single planar obstacle.

5. Reconstruction of the material parameters of a single obstacle. Once the position x_1 of a domain Ω_1 is known, one can easily determine the polarizations $p_1(\omega_n)$ of (3.1), (3.2) for each probing frequency ω_n with a least-squares fit to the given data. Assuming again for simplicity that $\nabla u_{\mathbb{1}}(x_1)$ is aligned with e_1, this means that

$$\frac{1}{|\nabla u_{\mathbb{1}}(x_1)|}\,p_1(\omega_n) = \begin{bmatrix} M_{11}\big(\lambda^{(1)}(\omega_n);\mathcal{O}_1\big) \\ M_{21}\big(\lambda^{(1)}(\omega_n);\mathcal{O}_1\big) \end{bmatrix} \tag{5.1}$$

is computable from the given data.

The following definition will prove useful.

Definition 5.1. *A bounded and simply connected planar shape $\mathcal{O} \subset \mathbb{R}^2$ is called* critical, *if its polarization tensor $M(\lambda;\mathcal{O})$ is a diagonal matrix for all $\lambda \in \widehat{\mathbb{C}}$ and its diagonal entries are rational functions of λ.*

We mention that the only examples of critical shapes, that we are aware of, are ellipses aligned with the coordinate axes.

Theorem 5.2. *If $\mathcal{O}_1$ is not critical in the sense of Definition 5.1 then the dipole moments (5.1) for infinitely many frequencies $\omega_n \in (0,\infty)$, $n \in \mathbb{N}$, uniquely determine the conductivity σ_1 and the permittivity ε_1 of the obstacle Ω_1.*

Proof. As in the proof of Theorem 4.1 we make use of the fact that the right-hand side of (5.1) is a meromorphic function of $\omega \in \widehat{\mathbb{C}} \setminus \{(1+\sigma_1)\mathrm{i}/\varepsilon_1\}$. Thus, by analytic continuation we can assume that the function

$$t \;\mapsto\; F(t) = M_{11}\big(\lambda^{(1)}(\mathrm{i}t);\mathcal{O}_1\big) \tag{5.2}$$

is at our disposal. Note that "imaginary frequencies" $\omega = \mathrm{i}t$ correspond to real values of $\lambda = \lambda^{(1)}(\omega)$ by virtue of (4.2) and that the map $\lambda \mapsto t = \omega^{(1)}(\lambda)/\mathrm{i}$ is strictly monotonically decreasing over $\mathbb{R}$ (except for its pole at $\lambda = -1/2$), mapping the three values

$$\lambda = -1/2,\ 0,\ 1/2 \qquad \text{onto} \qquad t = \pm\infty,\ (\sigma_1+1)/\varepsilon_1,\ \sigma_1/\varepsilon_1 > 0\,,$$

in this respective order.

Since the top left entry $M_{11}(\lambda;\mathcal{O}_1)$ of the polarization tensor is a strictly monotonic function of $\lambda \in \widehat{\mathbb{R}} = \mathbb{R} \cup \{\pm\infty\}$ (except for its poles), with $\lambda = \pm\infty$ being its only roots in

the exterior of $[-1/2, 1/2]$, the real-valued function F of (5.2) has a unique root $t_0 < \sigma_1/\varepsilon_1$, namely,

$$t_0 = \frac{1}{\mathrm{i}}\,\omega^{(1)}(\pm\infty) = \frac{\sigma_1 - 1}{\varepsilon_1}\,. \tag{5.3}$$

We now distinguish the two cases of whether the function F has infinitely many poles, or not. If F has infinitely many poles then these poles necessarily cluster at

$$t_\infty = \frac{1}{\mathrm{i}}\,\omega^{(1)}(0) = \frac{\sigma_1 + 1}{\varepsilon_1}\,,$$

because these poles correspond to Fredholm eigenvalues λ_k of $\mathcal{O}_1$, which can only cluster at $\lambda = 0$. Obviously, given t_0 and t_∞, it follows that

$$\varepsilon_1 = \frac{2}{t_\infty - t_0} \qquad \text{and} \qquad \sigma_1 = \frac{t_\infty + t_0}{t_\infty - t_0}\,.$$

On the other hand, if F has only finitely many poles then t_∞ cannot be determined from the given data, and we have to proceed differently. In fact, in this case we utilize that $M_{21}(\cdot\,;\mathcal{O}_1)$ cannot vanish identically, for otherwise $\mathcal{O}_1$ were critical in the sense of Definition 5.1. But then $M_{21}(\cdot\,;\mathcal{O}_1)$ must have poles by virtue of (2.7) and, because of its symmetry, we may denote the two poles with maximum absolute value by $\pm\lambda_1 \in (-1/2, 1/2)$. Because of the monotonicity of the map $\lambda \mapsto t$ the corresponding numbers

$$t_{\pm 1} = \frac{1}{\mathrm{i}}\,\omega^{(1)}(\pm\lambda_1)$$

are the extremal poles of F and, hence, these two numbers can be determined from the data again. It follows that

$$\frac{1 + \sigma_1 - t_{-1}\varepsilon_1}{1 - \sigma_1 + t_{-1}\varepsilon_1} = 2\lambda^{(1)}(\mathrm{i}t_{-1}) = -2\lambda^{(1)}(\mathrm{i}t_1) = -\frac{1 + \sigma_1 - t_1\varepsilon_1}{1 - \sigma_1 + t_1\varepsilon_1}\,,$$

and making use of (5.3) we can uniquely solve for

$$\varepsilon_1 = \frac{t_1 + t_{-1} - 2t_0}{(t_{-1} - t_0)(t_1 - t_0)} \qquad \text{and} \qquad \sigma_1 = \frac{t_{-1}t_1 - t_0^2}{(t_{-1} - t_0)(t_1 - t_0)}\,.$$

Thus, in either case we can determine both material parameters from the data. ∎

We mention that even for a critical shape the ratio (5.3) is determined by the corresponding multifrequency data. Thus, knowing either ε_1 or σ_1, the other parameter can be computed from (5.3). On the other hand, if neither ε_1 nor σ_1 are known, then there are examples where the material parameters *cannot* be determined.

Theorem 5.3. *If two obstacles Ω_1 and $\widetilde{\Omega}_1$ have critical shapes $\mathcal{O}_1$ and $\widetilde{\mathcal{O}}_1$ and material parameters ε_1, σ_1 and $\widetilde{\varepsilon}_1$, $\widetilde{\sigma}_1$, respectively, and yield the same dipole moments (5.1) for infinitely many frequencies $\omega_n \in (0, \infty)$, then the polynomial*

$$q(\lambda) = \frac{\varepsilon_1}{\widetilde{\varepsilon}_1}\,\lambda - \frac{1}{2}\left(1 - \frac{\varepsilon_1}{\widetilde{\varepsilon}_1}\right) \tag{5.4}$$

provides a one-to-one correspondence of the poles of $M_{11}(\cdot;\mathcal{O}_1)$ *with those of* $M_{11}(\cdot;\widetilde{\mathcal{O}}_1)$*: If* λ *is a pole of* $M_{11}(\cdot;\mathcal{O}_1)$ *then* $q(\lambda)$ *is a pole of* $M_{11}(\cdot;\widetilde{\mathcal{O}}_1)$*, and vice versa.*

Proof. Since the derivation of (5.3) in the proof of the preceding theorem is independent of whether the shape of the obstacle is critical or not, we find that under the present assumptions there is a unique number t_0 such that

$$t_0 = \frac{\sigma_1 - 1}{\varepsilon_1} = \frac{\widetilde{\sigma}_1 - 1}{\widetilde{\varepsilon}_1}\,. \tag{5.5}$$

On the other hand there holds

$$M_{11}\big(\lambda^{(1)}(\omega_n);\mathcal{O}_1\big) = M_{11}\big(\widetilde{\lambda}^{(1)}(\omega_n);\widetilde{\mathcal{O}}_1\big) \qquad \text{for all } n \in \mathbb{N}\,,$$

where $\widetilde{\lambda}^{(1)}(\omega)$ is defined as in (2.6), replacing σ_l and ε_l by $\widetilde{\sigma}_1$ and $\widetilde{\varepsilon}_1$, respectively. Since $\lambda^{(1)}$ is a bijective Möbius transformation of the complex plane (cf. (2.6)) this can be rewritten as

$$M_{11}(\lambda;\mathcal{O}_1) = M_{11}\big(q(\lambda);\widetilde{\mathcal{O}}_1\big) \tag{5.6}$$

for all $\lambda = \lambda^{(1)}(\omega_n)$, $n \in \mathbb{N}$, where

$$\begin{aligned} q(\lambda) &= \widetilde{\lambda}^{(1)}\big(\omega^{(1)}(\lambda)\big) \\ &= \frac{1}{2}\,\frac{(2\varepsilon_1 + 2\varepsilon_1\widetilde{\sigma}_1 + 2\widetilde{\varepsilon}_1 - 2\widetilde{\varepsilon}_1\sigma_1)\lambda + \varepsilon_1 + \varepsilon_1\widetilde{\sigma}_1 - \widetilde{\varepsilon}_1 - \widetilde{\varepsilon}_1\sigma_1}{(2\varepsilon_1 - 2\varepsilon_1\widetilde{\sigma}_1 - 2\widetilde{\varepsilon}_1 + 2\widetilde{\varepsilon}_1\sigma_1)\lambda + \varepsilon_1 - \varepsilon_1\widetilde{\sigma}_1 + \widetilde{\varepsilon}_1 + \widetilde{\varepsilon}_1\sigma_1}\,, \end{aligned} \tag{5.7}$$

with $\omega^{(1)}$ of (4.2) being the inverse function of $\lambda^{(1)}$ again. Since the sequence $\lambda^{(1)}(\omega_n)$, $n \in \mathbb{N}$, clusters at some $\lambda \in \widehat{\mathbb{C}}$ it follows from the uniqueness theorem for rational functions that the validity of (5.6) extends to all $\lambda \in \widehat{\mathbb{C}}$.

Inserting (5.5) into (5.7) the Möbius transformation q simplifies to the polynomial stated in (5.4) and, hence, the assertion of the theorem follows from (5.6). ∎

Although Theorem 5.3 only provides a necessary condition for a nonunique determination of the material parameters, this condition is quite strong. We are aware of only one class of examples where it is met, and this class does indeed provide a nonuniqueness case.

Example 5.4. Consider an ellipse $\Omega_1 = x_1 + \delta\mathcal{O}_1$ at x_1 such that $\mathcal{O}_1$ has half axes of lengths $\delta_2 \neq \delta_1$, the latter being aligned with $\nabla u_{\mathbb{1}}(x_1)$ and the first standard basis vector e_1. Then there holds

$$p_1(\omega_n) = M\big(\lambda^{(1)}(\omega_n);\mathcal{O}_1\big)\nabla u_{\mathbb{1}}(x_1) = \frac{|\mathcal{O}_1|}{\lambda^{(1)}(\omega_n) - \lambda_{\mathcal{E}}}\,\nabla u_{\mathbb{1}}(x_1)$$

with $\lambda^{(1)}$ of (2.6) and $\lambda_{\mathcal{E}}$ of (2.9). As before, σ_1 and ε_1 denote the material parameters of this ellipse.

On the other hand, let $\widetilde{\Omega}_1 = x_1 + \delta\widetilde{\mathcal{O}}_1$ be a disk-shaped obstacle at x_1 with permittivity

$$\widetilde{\varepsilon}_1 = \frac{2\delta_2}{\delta_1 + \delta_2}\,\varepsilon_1 \;\neq\; \varepsilon_1 \tag{5.8}$$

and conductivity

$$\widetilde{\sigma}_1 = 1 + \frac{\varepsilon_2}{\varepsilon_1}(\sigma_1 - 1)\,, \tag{5.9}$$

such that (5.5) is satisfied. Assuming that

$$|\widetilde{\mathcal{O}}_1| = \frac{\delta_1 + \delta_2}{2\delta_2}\,|\mathcal{O}_1|\,,$$

the resulting dipole moments

$$\widetilde{p}_1(\omega_n) = M\big(\widetilde{\lambda}^{(1)}(\omega_n); \mathcal{O}_2\big)\nabla u_{\mathbb{1}}(x_1) = \frac{|\widetilde{\mathcal{O}}_1|}{\widetilde{\lambda}^{(1)}(\omega_n)}\,\nabla u_{\mathbb{1}}(x_1)$$

coincide with $p_1(\omega_n)$, because it is straightforward to check using (5.8), (5.9), and (2.9) that

$$\widetilde{\lambda}^{(1)}(\omega_n) = \frac{1}{2}\frac{1 + \widetilde{\sigma}_1 + \mathrm{i}\omega\widetilde{\varepsilon}_1}{1 - \widetilde{\sigma}_1 - \mathrm{i}\omega\widetilde{\varepsilon}_1} = \frac{\delta_1 + \delta_2}{2\delta_2}\big(\lambda^{(1)}(\omega_n) - \lambda_{\mathcal{E}}\big)\,.$$

Thus, it is impossible to decide from the given data which of the two material parameter pairs is the correct one. Obviously, we cannot determine the shape of the obstacle, either. ■

Remark 5.5. On the positive side we mention that if the material parameters are known (or can be determined as described in the proof of Theorem 5.2) then the reconstructed dipole moments (5.1) provide by analytic continuation the first column of the polarization tensor of $\mathcal{O}_1$ as a function of $\lambda \in \widehat{\mathbb{C}} \setminus \{0\}$. By virtue of (2.7) we can go on and determine the second column from the first one. Thus we know the full polarization tensor as a function of λ in this case.

As mentioned in section 2 we can conclude from this that the shape of the present obstacle belongs to a certain equivalence class of shapes—it may even be uniquely determined this way up to rotations by π. ■

6. Reconstruction of the positions of two obstacles and the multifrequency MUSIC scheme. In what follows we turn our attention to the situation where two small obstacles Ω_1 and Ω_2 are present in $\mathcal{D}$. We start with an example to show that the reconstruction of their two positions may run into problems when the traditional MUSIC algorithm is used for AC data as introduced in section 3. We will propose a slightly improved algorithm below, the *multifrequency MUSIC scheme*, that will not fail in some of these cases.

Example 6.1. Consider two geometrically similar ellipses $\mathcal{O}_1$ and $\mathcal{O}_2$ with identical material parameters and areas ρ^2 and σ^2, respectively, where one of the half axes of $\mathcal{O}_1$ is parallel to $\nabla u_{\mathbb{1}}(x_1) = |\nabla u_{\mathbb{1}}(x_1)|e_1$, whereas the corresponding half axis of $\mathcal{O}_2$ forms an angle $\varphi \in (-\pi/2, \pi/2) \setminus \{0\}$ to $\nabla u_{\mathbb{1}}(x_2)$ (cf. Figure 1). Furthermore, we denote by α the angle between $\nabla u_{\mathbb{1}}(x_2)$ and e_1, i.e.,

$$\nabla u_{\mathbb{1}}(x_2) = |\nabla u_{\mathbb{1}}(x_2)|\,Q_\alpha e_1 = |\nabla u_{\mathbb{1}}(x_2)|\begin{bmatrix}\cos\alpha\\ \sin\alpha\end{bmatrix}, \tag{6.1}$$

where Q_α is the rotation matrix defined in (2.8).

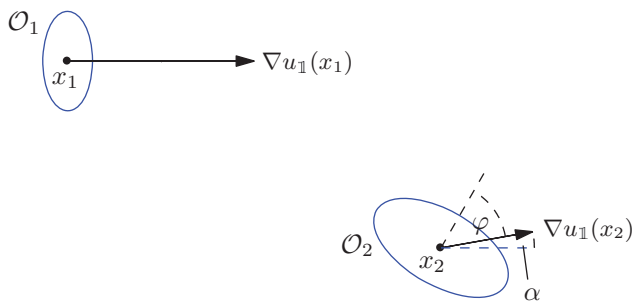

Figure 1. *Sketch of the geometrical setup of Example 6.1.*

The frequency ω_n translates into the spectral parameter $\lambda^{(1)}(\omega_n)$ of (2.6), such that

$$p_1(\omega_n) = |\nabla u_{\mathbb{1}}(x_1)|\,\rho^2 \begin{bmatrix} \dfrac{1}{\lambda^{(1)}(\omega_n) - \lambda_{\mathcal{E}}} \\ 0 \end{bmatrix}$$

for $\lambda_{\mathcal{E}}$ as in (2.9) (cf. Example 2.1), whereas

$$\begin{aligned} p_2(\omega_n) &= \frac{\sigma^2}{\rho^2}\, M\big(\lambda^{(1)}(\omega_n); Q_{\varphi+\alpha}(\mathcal{O}_1)\big)\nabla u_{\mathbb{1}}(x_2) \\ &= |\nabla u_{\mathbb{1}}(x_2)|\,\frac{\sigma^2}{\rho^2}\, Q_\alpha M\big(\lambda^{(1)}(\omega_n); Q_\varphi(\mathcal{O}_1)\big) e_1 \\ &= |\nabla u_{\mathbb{1}}(x_2)|\,\sigma^2 \begin{bmatrix} \dfrac{\cos\varphi\,\cos(\varphi+\alpha)}{\lambda^{(1)}(\omega_n) - \lambda_{\mathcal{E}}} + \dfrac{\sin\varphi\,\sin(\varphi+\alpha)}{\lambda^{(1)}(\omega_n) + \lambda_{\mathcal{E}}} \\ \dfrac{\cos\varphi\,\sin(\varphi+\alpha)}{\lambda^{(1)}(\omega_n) - \lambda_{\mathcal{E}}} - \dfrac{\sin\varphi\,\cos(\varphi+\alpha)}{\lambda^{(1)}(\omega_n) + \lambda_{\mathcal{E}}} \end{bmatrix} \end{aligned}$$

according to (2.10) and (6.1). It thus follows that

$$p_1(\omega_n) = \frac{|\nabla u_{\mathbb{1}}(x_1)|}{|\nabla u_{\mathbb{1}}(x_2)|}\,\frac{\rho^2}{\sigma^2}\,\frac{1}{\cos\varphi} \begin{bmatrix} \cos(\varphi+\alpha) & \sin(\varphi+\alpha) \\ 0 & 0 \end{bmatrix} p_2(\omega_n) \tag{6.2}$$

for all $n \in \mathbb{N}$.

In order to simplify the notation in (6.2) we denote the factor in front of $p_2(\omega_n)$ by $X_{12} \in \mathbb{R}^{2\times 2}$. Then, for any $\boldsymbol{a} \in \ell^1$ there holds (cf. (3.5))

$$A_\circ \boldsymbol{a} = \left(X_{12} \left(\sum_{n=1}^{\infty} a_n p_2(\omega_n) \right) \right) \cdot \nabla_z N(\cdot, x_1)\big|_\Gamma + \left(\sum_{n=1}^{\infty} a_n p_2(\omega_n) \right) \cdot \nabla_z N(\cdot, x_2)\big|_\Gamma\,,$$

and it follows that the test function $\phi_{z,p}$ of (3.3) with $z = x_1$ and *arbitrary* dipole moment $p \neq 0$ can never belong to the range of $A_\circ$ (cf. Proposition 3.1(b)). In addition, the corresponding

test function with $z = x_2$ can only belong to the range of $A_\circ$, if the test dipole moment p belongs to the null space of X_{12}, i.e., if

$$p = c \begin{bmatrix} \sin(\varphi + \alpha) \\ -\cos(\varphi + \alpha) \end{bmatrix} \qquad \text{for some } c \neq 0\,, \tag{6.3}$$

whereas the algorithm considered so far utilizes the dipole moment $p_{x_2} = \nabla u_{\mathbb{1}}(x_2)$ of (6.1), which is not collinear with the proper choice (6.3) of p, because $\varphi \neq \pm\pi/2$.

Since φ is assumed to be nonzero the test vector p of (6.3) can, indeed, be written as a linear combination of any two vectors $p_2(\omega_n)$ with different frequencies ω_n. ■

We conclude from Example 6.1 that for certain geometrical setups the MUSIC scheme considered so far is unable to determine either of the two objects whereas it is possible to find at least one of them when changing the algorithm in the following way.[2]

Algorithm 6.2 (multifrequency MUSIC scheme). *For a given test point $z \in \mathcal{D}$ check whether the test function $\phi_{z,p}$ of (3.3) does (approximately) belong to the range of A_δ for any (complex) dipole moment $p \in \mathbb{S}^1 = \{q \in \mathbb{C}^2 : |q| = 1\}$. When this is the case, the test point z is considered to be the (approximate) location of one of the obstacles.*

While this multifrequency MUSIC scheme is capable of localizing Ω_2 in Example 6.1 above, it still fails to localize Ω_1. Such a situation will be called a *weak failure* in the following; in contrast, a situation where neither of the two obstacles is found is considered a *fatal failure* below. Unfortunately it is quite easy to see that the multifrequency MUSIC scheme also cannot avoid fatal failures.

Example 6.3. Let Ω consist of two obstacles with geometrically similar shapes $\mathcal{O}_1$ and $\mathcal{O}_2$ and identical material parameters, located at x_1 and x_2, respectively, and let $Q \in \mathbb{R}^{2\times 2}$ be the orthogonal transformation such that

$$\mathcal{O}_1 = cQ(\mathcal{O}_2)\,, \qquad c = |\mathcal{O}_1|/|\mathcal{O}_2|\,.$$

From (2.10) we know that

$$M(\lambda; \mathcal{O}_1) = c^2 Q M(\lambda; \mathcal{O}_2) Q^*$$

for every $\lambda \in \mathbb{C}$. Assume further that the gradients of the reference potential $u_{\mathbb{1}}$ at x_1 and x_2 satisfy

$$\nabla u_{\mathbb{1}}(x_1) = \mu Q \nabla u_{\mathbb{1}}(x_2)$$

for some $\mu \in \mathbb{R}$ (cf. Figure 2). Then, with $\lambda^{(1)}(\omega) = \lambda^{(2)}(\omega) =: \lambda(\omega)$ (cf. (2.6)) it follows that

$$p_1(\omega) = M\big(\lambda(\omega); \mathcal{O}_1\big) \nabla u_{\mathbb{1}}(x_1) = c^2 Q M\big(\lambda(\omega); \mathcal{O}_2\big) Q^* \nabla u_{\mathbb{1}}(x_1) = \mu c^2 Q p_2(\omega)$$

for every $\omega > 0$ and, hence, criterion (3.6) can only hold for either $l = 1$ or $l = 2$, when $p = 0$. In other words, neither of the two obstacles will be detected by the multifrequency MUSIC scheme.

Of course, the same conclusion applies if $\mathcal{O}_1$ and $cQ(\mathcal{O}_2)$ are merely polarization equivalent in the sense of Definition 2.2. ■

[2] We admit that the authors of [1] do indeed test three different dipole moments in their numerical examples, namely, $p = p_z$ of (3.4) *and* the two standard basis vectors $p = e_1$ and $p = e_2$.

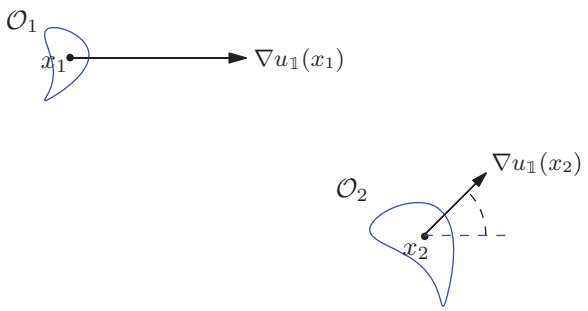

Figure 2. *Sketch of the geometrical setup of Example 6.3.*

Fatal failures of Algorithm 6.2 can only be avoided by testing linear combinations of dipoles located at different test points $z_1, z_2, \ldots$, spoiling the simplicity and elegance of the MUSIC scheme. To understand the likelihood of a fatal failure, we set up a complete list of all possible instances of fatal failures with $l_* = 2$ planar obstacles in what follows. As before, we assume that

$$\nabla u_{\mathbb{1}}(x_l) \neq 0\,, \qquad l = 1, 2\,,$$

and we restrict ourselves to the ideal situation of $n_* = \infty$ different probing frequencies.

To start with, we consider the case when the algorithm fails to detect the position x_1 of Ω_1. According to Proposition 3.1 this happens if and only if

$$\sum_{n=1}^{\infty} a_n p_2(\omega_n) = 0 \qquad \Longrightarrow \qquad \sum_{n=1}^{\infty} a_n p_1(\omega_n) = 0$$

for every $\boldsymbol{a} = [a_n] \in \ell^1$. Note that these two identities consist of two complex equations, each. Using [14, Lemma 4.14] again, the above implication is equivalent to the existence of a (possibly complex) 2×2 matrix X_{12} such that

$$p_1(\omega_n) = X_{12} p_2(\omega_n) \qquad \text{for all } n \in \mathbb{N}\,. \tag{6.4}$$

Without loss of generality let the coordinate system be such that

$$\nabla u_{\mathbb{1}}(x_1) = |\nabla u_{\mathbb{1}}(x_1)|\, e_1 \tag{6.5a}$$

is aligned with the first coordinate vector; moreover, let $Q \in \mathbb{R}^{2\times 2}$ be the rotation matrix for which

$$\nabla u_{\mathbb{1}}(x_2) = |\nabla u_{\mathbb{1}}(x_2)| Q^* e_1\,. \tag{6.5b}$$

Then, recalling (3.2) and using (2.10) again, relation (6.4) is equivalent to

$$\begin{aligned} |\nabla u_{\mathbb{1}}(x_1)| M\big(\lambda^{(1)}(\omega_n); \mathcal{O}_1\big)\, e_1 &= |\nabla u_{\mathbb{1}}(x_2)|\, X_{12} M\big(\lambda^{(2)}(\omega_n); \mathcal{O}_2\big) Q^* e_1 \\ &= |\nabla u_{\mathbb{1}}(x_2)|\, X_{12} Q^* M\big(\lambda^{(2)}(\omega_n); Q(\mathcal{O}_2)\big) e_1\,, \qquad n \in \mathbb{N}\,. \end{aligned} \tag{6.6}$$

As in the proof of Theorem 5.3 it follows that

$$M(\lambda;\mathcal{O}_1)e_1 = Y_{12}M\big(\Phi_{21}(\lambda);Q(\mathcal{O}_2)\big)e_1 \tag{6.7}$$

for all $\lambda \in \widehat{\mathbb{C}} \setminus \{0\}$, where

$$Y_{12} = \frac{|\nabla u_{\mathbb{1}}(x_2)|}{|\nabla u_{\mathbb{1}}(x_1)|}\, X_{12}Q^* \ \in \mathbb{C}^{2\times 2}$$

and

$$\begin{aligned}\Phi_{21}(\lambda) &= \lambda^{(2)}\big(\omega^{(1)}(\lambda)\big)\\ &= \frac{1}{2}\,\frac{(2\varepsilon_1 + 2\varepsilon_1\sigma_2 + 2\varepsilon_2 - 2\varepsilon_2\sigma_1)\lambda + \varepsilon_1 + \varepsilon_1\sigma_2 - \varepsilon_2 - \varepsilon_2\sigma_1}{(2\varepsilon_1 - 2\varepsilon_1\sigma_2 - 2\varepsilon_2 + 2\varepsilon_2\sigma_1)\lambda + \varepsilon_1 - \varepsilon_1\sigma_2 + \varepsilon_2 + \varepsilon_2\sigma_1}\,,\end{aligned} \tag{6.8}$$

similar to (5.7).

Note that when Y_{12} (resp., X_{12}) is nonsingular then there holds

$$p_2(\omega_n) = X_{21}p_1(\omega_n) \qquad \text{for all } n \in \mathbb{N} \tag{6.9}$$

with $X_{21} = X_{12}^{-1}$. On the other hand, some matrix X_{21} to satisfy (6.9) may exist even when X_{12} is singular. From what we have said before, (6.9) implies that x_2 will not be detected by the algorithm, either; in fact, the validity of (6.9) on top of (6.4) distinguishes fatal failures from weak failures.

To derive necessary and sufficient algebraic conditions for a weak (resp., fatal) failure of Algorithm 6.2 we need to consider the case that X_{12} is singular. By virtue of (2.7) $M_{11}(\cdot;\mathcal{O}_1)$ is not vanishing identically, and therefore the top row of X_{12} cannot be zero. Accordingly, if X_{12} is singular then its bottom row is a multiple of the top row and, hence, it follows from (6.6) that $M_{21}(\cdot;\mathcal{O}_1)$ is a multiple of $M_{11}(\cdot;\mathcal{O}_1)$. As has already been mentioned, though, the latter is a monotonically decreasing function of $\lambda \in \mathbb{R}$ (except for its poles), whereas M_{21} is a decreasing function of λ only when it is identically zero. We thus have shown that

$$M_{21}(\cdot;\mathcal{O}_1) = 0 \tag{6.10}$$

when X_{12} is singular.

A fatal failure, i.e., (6.9), implies similarly to (6.7) that

$$M\big(\lambda;Q(\mathcal{O}_2)\big)e_1 = Y_{21}M\big(\Phi_{21}^{-1}(\lambda);\mathcal{O}_1\big)e_1$$

for some $Y_{21} \in \mathbb{C}^{2\times 2}$ and all $\lambda \in \widehat{\mathbb{C}} \setminus \{0\}$. Hence, for a fatal failure with a singular matrix X_{12} there holds

$$M_{21}\big(\lambda;Q(\mathcal{O}_2)\big) = cM_{11}\big(\Phi_{21}^{-1}(\lambda);\mathcal{O}_1\big)$$

for some $c \in \mathbb{C}$ in view of (6.10). Using once again that the left-hand side of this equation is an even function of $\lambda \in \mathbb{R}$, whereas the right-hand side is a monotonic function of $\lambda \in \mathbb{R}$—take note that the Möbius transformation Φ_{21}^{-1} is also monotonic on $\mathbb{R}$—it follows that $M_{21}(\cdot;Q(\mathcal{O}_2))$ must also vanish identically. Therefore the singular matrix X_{12} in (6.6) can be replaced by a nonsingular multiple of Q without affecting the validity of (6.4) and (6.6).

Summarizing, we can state the following result.

Proposition 6.4. *Assuming the coordinate system of* $\mathbb{R}^2$ *to be such that* (6.5) *is valid, a fatal failure of Algorithm* 6.2 *occurs if and only if* (6.6) *holds true for some nonsingular matrix* X_{12}.

We will focus on fatal failures in what follows, before we return to weak failures in section 9, where we also show how to adapt the algorithm to overcome them.

7. Fatal failure of the multifrequency MUSIC scheme: Different material parameters.

We continue the analysis of fatal failures of the multifrequency MUSIC algorithm with $l_* = 2$ obstacles by assuming first that the material parameters of the two obstacles are different. Here we have the following result.

Theorem 7.1. *Under the assumption* (6.5) *two infinitesimal obstacles* Ω_1 *and* Ω_2 *as in* (2.4) *with different material parameters lead to a fatal failure of Algorithm* 6.2 *if and only if the following conditions are met:*

(i) *the material parameters of* Ω_1 *and* Ω_2 *satisfy*

$$\frac{\sigma_1 - 1}{\varepsilon_1} = \frac{\sigma_2 - 1}{\varepsilon_2}\,, \tag{7.1}$$

(ii) $\mathcal{O}_1$ *and* $Q(\mathcal{O}_2)$ *are both critical in the sense of Definition* 5.1,

(iii) *there holds*

$$M_{11}(\lambda; \mathcal{O}_1) = cM_{11}\big(q(\lambda); Q(\mathcal{O}_2)\big) \tag{7.2}$$

for all $\lambda \in \widehat{\mathbb{C}} \setminus \{0\}$ *and some* $c \in \mathbb{R} \setminus \{0\}$, *where*

$$q(\lambda) = \frac{\varepsilon_1}{\varepsilon_2}\,\lambda - \frac{1}{2}\left(1 - \frac{\varepsilon_1}{\varepsilon_2}\right)\,. \tag{7.3}$$

Proof. To begin with, assume that (i) to (iii) hold true. Then, because of (7.1), the polynomial q and Φ_{21} of (6.8) are seen to be identical. Moreover, since $\mathcal{O}_1$ and $Q(\mathcal{O}_2)$ are critical shapes their polarization tensors are diagonal ones and, hence, (7.2) implies that

$$M(\lambda; \mathcal{O}_1)e_1 = cM\big(\Phi_{21}(\lambda); Q(\mathcal{O}_2)\big)e_1$$

for all $\lambda \in \widehat{\mathbb{C}}$, so that (6.7) is valid with $Y_{12} = cI$. Because of the equivalence of (6.6) and (6.7), Algorithm 6.2 will thus encounter a fatal failure by virtue of Proposition 3.1.

Consider next a fatal failure of Algorithm 6.2, and denote by

$$\lambda_* = -\frac{1}{2}\,\frac{\varepsilon_1 - \varepsilon_1\sigma_2 + \varepsilon_2 + \varepsilon_2\sigma_1}{\varepsilon_1 - \varepsilon_1\sigma_2 - \varepsilon_2 + \varepsilon_2\sigma_1} \in \widehat{\mathbb{R}}$$

the pole of Φ_{21} of (6.8). Then there holds

$$M_{11}(\lambda_*, \mathcal{O}_1) = 0 \qquad \text{and} \qquad M_{11}\big(\Phi_{21}(\infty), Q(\mathcal{O}_2)\big) = 0\,, \tag{7.4}$$

where the first equality is an immediate consequence of (6.7), because the right-hand side of (6.7) vanishes when $\Phi_{21}(\lambda) = \Phi_{21}(\lambda_*) = \infty$, while the second statement of (7.4) can be

deduced from (6.7) because Y_{12} can be chosen nonsingular in the fatal failure case according to Proposition 6.4.

Using once again that $M_{11}(\lambda;\mathcal{O}_1)$ is a strictly decreasing function of $\lambda\in\mathbb{R}$ (except for its poles), with zero limit as $|\lambda|\to\infty$, it follows from (7.4) that either $\lambda_*=\infty$ (or, equivalently, that the Möbius transformation Φ_{21} is a polynomial), or that λ_* is enclosed by two poles of $M(\cdot;\mathcal{O}_1)$, i.e., by two Fredholm eigenvalues of $\mathcal{O}_1$. Since these eigenvalues are bounded by $1/2$ in absolute value, the latter implies that

$$|\lambda_*| = \frac{1}{2}\left|1+\frac{2\varepsilon_2}{\varepsilon_1(1-\sigma_2)+\varepsilon_2(\sigma_1-1)}\right| < \frac{1}{2}\,.$$

In other words, if Φ_{21} fails to be a polynomial then there holds

$$\varepsilon_1(1-\sigma_2)+\varepsilon_2(\sigma_1-1)<0\,. \tag{7.5}$$

On the other hand, the second statement of (7.4) implies in much the same way that either $\Phi_{21}(\infty)=\infty$, or

$$\big|\Phi_{21}(\infty)\big| = \frac{1}{2}\left|\frac{\varepsilon_1+\varepsilon_1\sigma_2+\varepsilon_2-\varepsilon_2\sigma_1}{\varepsilon_1-\varepsilon_1\sigma_2-\varepsilon_2+\varepsilon_2\sigma_1}\right| = \frac{1}{2}\left|1+\frac{2\varepsilon_1}{\varepsilon_1(\sigma_2-1)+\varepsilon_2(1-\sigma_1)}\right| < \frac{1}{2}\,,$$

in contradiction to (7.5). Thus there holds $\Phi_{21}(\infty)=\infty$, i.e., Φ_{21} is a first order polynomial, and by virtue of (6.8) this is the case if and only if the material parameters of $\mathcal{O}_1$ and $\mathcal{O}_2$ are connected via (7.1). This proves (i).

Inserting (7.1) into (6.8), Φ_{21} is seen to coincide with q of (7.3) (similar to (5.4)). Note that

$$q(0)\;\neq\;0 \tag{7.6}$$

for otherwise $\varepsilon_1=\varepsilon_2$ and, hence, $\sigma_1=\sigma_2$ by virtue of (7.1), contradicting our assumption that the material parameters of Ω_1 and Ω_2 are different,

Consider now $M_{21}(\cdot;\mathcal{O}_1)$. Because of (2.7), $M_{21}(\lambda;\mathcal{O}_1)$ decays like $O(|\lambda|^{-2})$ as $|\lambda|$ goes to infinity, whereas the right-hand side of (6.7) only decays that fast near infinity, when the bottom left entry of Y_{12} is zero, i.e., if

$$M_{21}(\lambda;\mathcal{O}_1) = cM_{21}\big(q(\lambda);Q(\mathcal{O}_2)\big)$$

for some $c\neq 0$ and all $\lambda\in\widehat{\mathbb{C}}\setminus\{0\}$ (remember that Φ_{21} has been shown to coincide with q and that Y_{12} is nonsingular). Thus, if $M_{21}(\cdot;\mathcal{O}_1)$ is not identically zero then (2.7) and the monotonicity of q imply that the two poles of maximum absolute value, $\pm\lambda_1$ say, of $M_{21}(\cdot;\mathcal{O}_1)$ yield the extremal two poles $q(\pm\lambda_1)$ of $M_{21}(\cdot;Q(\mathcal{O}_2))$; however, as the latter also have to be symmetric to the origin, this contradicts (7.6), proving that $M_{21}(\cdot;\mathcal{O}_1)$ and $M_{21}(\cdot;Q(\mathcal{O}_2))$ must vanish identically. Inserting this back into (6.7), we have established (iii).

In order to prove that $\mathcal{O}_1$ and $Q(\mathcal{O}_2)$ are critical, it remains to show that $M_{11}(\cdot;\mathcal{O}_1)$ and $M_{11}(\cdot;Q(\mathcal{O}_2))$ can only have finitely many poles. If one of these two functions had infinitely many poles then these poles would (only) accumulate at the origin because of the compactness

of the double layer integral operator; moreover, by virtue of (7.2) the same had to be true for the other function, and the two accumulation points of the corresponding poles had to coincide. This, however, contradicts (7.6), and the proof is done. ∎

Note that the three requirements of Theorem 7.1 are exactly the conditions which prevent an identification of the material parameters of a single object (cf. section 5). As such, a very similar setting to Example 5.4 can be used to construct a situation where such a fatal failure occurs.

Example 7.2. Let Ω_1 and Ω_2 have the shapes and material parameters, respectively, as Ω_1 and $\widetilde{\Omega}_1$ in Example 5.4, but different locations $x_2 \neq x_1$ in $\mathcal{D}$. Assume furthermore that $\nabla u_{\mathbb{1}}(x_2)$ is collinear with $\nabla u_{\mathbb{1}}(x_1)$. As in Example 5.4 it then follows that

$$p_2(\omega_n) = \pm \frac{|\nabla u_{\mathbb{1}}(x_2)|}{|\nabla u_{\mathbb{1}}(x_1)|}\, p_1(\omega_n)$$

for all probing frequencies ω_n, $n \in \mathbb{N}$ and, hence, for either $l = 1$ or $l = 2$, criterion (3.6) can only hold when $p = 0$; in other words, neither of the two obstacles will be detected by the multifrequency MUSIC scheme. ∎

8. Fatal failure of the multifrequency MUSIC scheme: Identical material parameters.

We return to the necessary and sufficient criterion (6.6) for a fatal failure of Algorithm 6.2, with X_{12} being nonsingular by virtue of Proposition 6.4. On top of that we now make the assumption that the material parameters of the two obstacles are the same, i.e., that (6.7) holds true with Φ_{21} being the identity.

Consider first the case that $M_{21}(\cdot;\mathcal{O}_1)$ is identically zero. Then it follows from (6.7) that $M_{21}(\cdot;Q(\mathcal{O}_2))$ is a multiple of $M_{11}(\cdot;Q(\mathcal{O}_2))$ because Y_{12} is nonsingular, and using once more the monotonicity of M_{11} and the symmetry of M_{21} this can only be true when $M_{21}(\cdot;Q(\mathcal{O}_2))$ is also vanishing. Accordingly, with this assumption (6.6) implies that

$$M_{11}(\cdot;\mathcal{O}_1) = c^2 M_{11}\big(\cdot;Q(\mathcal{O}_2)\big)$$

for some $c \in \mathbb{R} \setminus \{0\}$ (the positivity of the factor c^2 is due to the monotonicity of M_{11}). Together with (2.7) and (2.10) this leads to

$$M(\cdot;\mathcal{O}_1) = c^2 M\big(\cdot;Q(\mathcal{O}_2)\big) = c^2 Q M(\cdot;\mathcal{O}_2) Q^*\,,$$

i.e., $\mathcal{O}_1$ and $cQ(\mathcal{O}_2)$ are polarization equivalent in the sense of Definition 2.2, and—recalling our standing assumption (6.5)—the two obstacles fulfill the standard case of a fatal failure as presented in Example 6.3.

Consider next the other case, where $M_{21}(\cdot;\mathcal{O}_1)$ is not identically zero. Then we can choose any symmetric pair $\pm\lambda_k$ of poles of $M_{21}(\cdot;\mathcal{O}_1)$, and conclude from (6.7) and (2.7) that for $\lambda \to \lambda_k$ there holds

$$\begin{aligned} r_k \begin{bmatrix} r_k \\ c_k r_{-k} \end{bmatrix} \frac{1}{\lambda - \lambda_k} \;&\sim\; M(\lambda;\mathcal{O}_1) e_1 = Y_{12} M(\lambda;Q(\mathcal{O}_2)) e_1 \\ &\sim\; s_k Y_{12} \begin{bmatrix} s_k \\ \tilde{c}_k s_{-k} \end{bmatrix} \frac{1}{\lambda - \lambda_k} \end{aligned} \tag{8.1}$$

with $c_k r_k r_{-k} \neq 0$ and corresponding residues $s_{\pm k}^2$ and associated parameter $\tilde{c}_k \in [0,1]$ of the polarization tensor of $Q(\mathcal{O}_2)$ in (2.7). We thus necessarily have $s_k \neq 0$ and

$$Y_{12} \begin{bmatrix} s_k \\ \tilde{c}_k s_{-k} \end{bmatrix} = \frac{r_k}{s_k} \begin{bmatrix} r_k \\ c_k r_{-k} \end{bmatrix}. \tag{8.2a}$$

A corresponding expansion for $\lambda \to -\lambda_k$ reveals that s_{-k} cannot vanish, either, and that

$$Y_{12} \begin{bmatrix} s_{-k} \\ -\tilde{c}_k s_k \end{bmatrix} = \frac{r_{-k}}{s_{-k}} \begin{bmatrix} r_{-k} \\ -c_k r_k \end{bmatrix}. \tag{8.2b}$$

Note that the right-hand sides of (8.2) are linearly independent; accordingly, the two vector arguments on the left must be linearly independent, too, excluding thus the option of $\tilde{c}_k$ being zero. Introducing the positive numbers

$$\rho_k = (r_k^2 + r_{-k}^2)^{1/2} \qquad \text{and} \qquad \sigma_k = (s_k^2 + s_{-k}^2)^{1/2}$$

we rewrite the residues as

$$\begin{aligned} r_k &= \rho_k \cos\theta_k\,, & r_{-k} &= \rho_k \sin\theta_k\,, \\ s_k &= \sigma_k \cos\varphi_k\,, & s_{-k} &= \sigma_k \sin\varphi_k\,, \end{aligned} \tag{8.3}$$

with $\theta_k \in (0, \pi/2)$ and $\varphi_k \in (-\pi/2, \pi/2) \setminus \{0\}$. Note that θ_k can be chosen from the interval $(-\pi/2, \pi/2)$, because only the products r_k^2, $r_k r_{-k}$, and r_{-k}^2 enter into the polarization tensor, and the same applies to φ_k; the additional restriction $\theta_k > 0$ can be stipulated without loss of generality, for we can always exchange λ_k and $-\lambda_k$ when necessary.

The (nonsingular) matrix Y_{12} of (8.1) is completely specified by means of (8.2), namely,

$$Y_{12} = c^2 \begin{bmatrix} 1 & \eta \\ 0 & \zeta \end{bmatrix} \tag{8.4}$$

with

$$c = \frac{\rho_k}{\sigma_k}\,, \qquad \eta = \frac{\cos(2\theta_k) - \cos(2\varphi_k)}{\tilde{c}_k \sin(2\varphi_k)}\,, \qquad \text{and} \qquad \zeta = \frac{c_k \sin(2\theta_k)}{\tilde{c}_k \sin(2\varphi_k)}\,; \tag{8.5}$$

notably, c, η, and ζ are independent of the particular pole λ_k of $M_{21}(\cdot;\mathcal{O}_1)$ that has been chosen.

From this stage onwards we confine ourselves to shapes $\mathcal{O}_l$, $l = 1, 2$, which are *simple* in the following sense.

Definition 8.1. *A planar bounded and simply connected C^2-smooth shape $\mathcal{O} \subset \mathbb{R}^2$ is called* simple *if all its nonzero Fredholm eigenvalues are simple.*

We recall from [9] that for a simple shape $\mathcal{O}$ the coefficients c_k in (2.7) can be omitted, since they are all equal to one (note that our normalization of the off-diagonal terms of the polarization tensor (2.7) is slightly different from the one in [9]).

Under this additional assumption that the two shapes are simple, if $\eta = 0$ in (8.5) then $\varphi_k = \pm\theta_k$ and $\zeta = \pm 1$. Thus (8.4) becomes

$$Y_{12} = c^2 Q^- \qquad \text{with} \qquad Q^- = \begin{bmatrix} 1 & 0 \\ 0 & \pm 1 \end{bmatrix},$$

i.e., Q^- corresponds to the identity or to the reflection at e_1. In either case (6.7) and (2.10) imply

$$M(\cdot;\mathcal{O}_1)e_1 = c^2 Q^- M\big(\cdot;Q(\mathcal{O}_2)\big)e_1 = M\big(\cdot;cQ'(\mathcal{O}_2)\big)e_1$$

with

$$Q' = Q^- \circ Q\,, \tag{8.6}$$

and (2.7) implies that $\mathcal{O}_1$ is polarization equivalent to $cQ'(\mathcal{O}_2)$. Since also

$$\nabla u_{\mathbb{1}}(x_1) = Q^- \nabla u_{\mathbb{1}}(x_1) = \mu Q' \nabla u_{\mathbb{1}}(x_2)$$

for some $\mu > 0$ by virtue of (6.5), this fatal failure is therefore another instance of the case presented in Example 6.3.

It remains to investigate the case $\eta \neq 0$ in (8.4) and (8.5). To this end we note that, proceeding as above, we obtain for *any* pole $\lambda_k \neq 0$ of the first column of $M(\cdot;\mathcal{O}_1)$ from (2.7) the corresponding analog of (8.1). Hence, either $r_{-k} = s_{-k} = 0$, or the analog of (8.2) holds true (note that $s_k \neq 0$ by virtue of (8.1), for otherwise λ_k is not a pole of $M(\cdot;Q(\mathcal{O}_2))e_1$). The latter case leads to the same representation of r_k, r_{-k}, s_k, and s_{-k} as in (8.3) with $\rho_k, \sigma_k > 0$, $\theta_k \in (0, \pi/2)$, and $\varphi_k \in (-\pi/2, \pi/2) \setminus \{0\}$ fulfilling (8.5) again. Note that for a simple shape (8.5) yields

$$\sin(2\theta_k) = \zeta \sin(2\varphi_k)\,, \qquad \cos(2\theta_k) = \eta \sin(2\varphi_k) + \cos(2\varphi_k)\,, \tag{8.7}$$

and turning to squares we obtain

$$(\eta^2 + \zeta^2 - 1)\sin^2(2\varphi_k) = -2\eta \sin(2\varphi_k)\cos(2\varphi_k)\,.$$

Since $\zeta \neq 0$ because of (8.5), it follows readily that

$$\cot(2\varphi_k) = \frac{1 - \xi^2 - \eta^2}{2\eta} \qquad \text{and} \qquad \cot(2\theta_k) = \frac{1 - \xi^2 + \eta^2}{2\eta\zeta}\,.$$

Thus, using the fact that $2\theta_k \in (0, \pi)$, we conclude that

$$\theta_k = \theta = \frac{1}{2}\operatorname{arccot}\frac{1 - \zeta^2 + \eta^2}{2\eta\zeta}\,, \tag{8.8a}$$

whereas

$$\varphi_k = \varphi = \begin{cases} \dfrac{1}{2}\operatorname{arccot}\dfrac{1 - \zeta^2 - \eta^2}{2\eta}\,, & \zeta > 0\,, \\[2ex] \dfrac{1}{2}\operatorname{arccot}\dfrac{1 - \zeta^2 - \eta^2}{2\eta} - \dfrac{\pi}{2}\,, & \zeta < 0\,, \end{cases} \tag{8.8b}$$

depending on the sign of ζ because of (8.7).

In other words, if $\eta \neq 0$ in (8.4) then the nonzero poles of $M(\cdot;\mathcal{O}_1)$ are the same as those of $M(\cdot;Q(\mathcal{O}_2))$, and the residues are determined by (8.3), where $\rho_k/\sigma_k = c$ is the same for all poles, and the angles θ_k and φ_k are either zero (corresponding to $r_{-k} = s_{-k} = 0$), or are given by (8.8). We gather the positive indices of the latter poles in an index set N_1, and those of the former ones in N_2. Subtracting off all these nonzero poles of $M(\cdot;\mathcal{O}_1)e_1$ and $M(\cdot;Q(\mathcal{O}_2))e_1$ we conclude from (6.7) and (8.4) that if $\lambda_k = 0$ is present in the expansion of $M_{11}(\cdot;\mathcal{O}_1)$ then it must also be present in $M_{11}(\cdot;Q(\mathcal{O}_2))$, and vice versa, and the residues must be given by $r_k^2 = \rho_k^2$ and $s_k^2 = \rho_k^2/c^2$, respectively; we thus include the corresponding index in N_2. Then it is not difficult to see that we can rewrite

$$M(\lambda;\mathcal{O}_1) = Q_\theta \begin{bmatrix} \sum_{k\in N_1} \frac{\rho_k^2}{\lambda-\lambda_k} & 0 \\ 0 & \sum_{k\in N_1} \frac{\rho_k^2}{\lambda+\lambda_k} \end{bmatrix} Q_\theta^* + \begin{bmatrix} \sum_{k\in N_2} \frac{\rho_k^2}{\lambda-\lambda_k} & 0 \\ 0 & \sum_{k\in N_2} \frac{\rho_k^2}{\lambda+\lambda_k} \end{bmatrix} \tag{8.9a}$$

and

$$M\big(\lambda;cQ(\mathcal{O}_2)\big) = Q_\varphi \begin{bmatrix} \sum_{k\in N_1} \frac{\rho_k^2}{\lambda-\lambda_k} & 0 \\ 0 & \sum_{k\in N_1} \frac{\rho_k^2}{\lambda+\lambda_k} \end{bmatrix} Q_\varphi^* + \begin{bmatrix} \sum_{k\in N_2} \frac{\rho_k^2}{\lambda-\lambda_k} & 0 \\ 0 & \sum_{k\in N_2} \frac{\rho_k^2}{\lambda+\lambda_k} \end{bmatrix} \tag{8.9b}$$

with $\rho_k > 0$ and the rotation matrices Q_θ and Q_φ (cf. (2.8)); here $\varphi \neq \pm\theta$ because $\eta \neq 0$. Note that N_1 is nonempty by construction, but N_2 can be the empty set.

Theorem 8.2. *Let Ω_l, $l = 1, 2$, be two infinitesimal obstacles at $x_l \in \mathcal{D}$ with identical material parameters and simple shapes $\mathcal{O}_l$ in the sense of Definition 8.1. Moreover, let the background potential satisfy (6.5) for some rotation Q, and define Q' by (8.6). If $\mathcal{O}_1/|\mathcal{O}_1|$ is neither polarization equivalent to $Q(\mathcal{O}_2)/|\mathcal{O}_2|$ nor to $Q'(\mathcal{O}_2)/|\mathcal{O}_2|$ then Algorithm 6.2 will encounter a fatal failure if and only if the polarization tensors of $\mathcal{O}_1$ and $Q(\mathcal{O}_2)$ satisfy (8.9) for appropriate values $c > 0$, $\theta \in (0, \pi/2)$, and $\varphi \in (-\pi/2, \pi/2) \setminus \{0\}$ with $|\varphi| \neq \theta$, where $N_1, N_2 \subset \mathbb{N}$ with $N_1 \neq \emptyset$ and $N_1 \cap N_2 = \emptyset$. Here, $\{|\lambda_k| : k \in N_1 \cup N_2\} \subset [0, 1/2)$ is a sequence of pairwise different Fredholm eigenvalues of $\mathcal{O}_1$ and $\mathcal{O}_2$ that may only cluster at the origin, and the sequence $\{\rho_k\} \subset (0, \infty)$ determines the corresponding residues.*

Proof. We have already proved the necessity of (8.9) for a fatal failure of the algorithm. On the other hand, it is easy to check that $M(\cdot;\mathcal{O}_1)$ and $M(\cdot;Q(\mathcal{O}_2))$ of (8.9) satisfy (6.7) with Y_{12} defined in (8.4), (8.5), where $c_k = \tilde{c}_k = 1$. Since (6.7) and (6.6) are equivalent, the other direction of the theorem thus follows from Proposition 6.4. ∎

An interesting special case of this theorem arises when $N_2 = \emptyset$. For any reference shape $\mathcal{O}$ whose polarization tensor has the form

$$M(\lambda;\mathcal{O}) = \begin{bmatrix} \sum_{k\in\mathbb{N}} \frac{\rho_k^2}{\lambda-\lambda_k} & 0 \\ 0 & \sum_{k\in\mathbb{N}} \frac{\rho_k^2}{\lambda+\lambda_k} \end{bmatrix}, \tag{8.10}$$

where $\{|\lambda_k| : k \in \mathbb{N}\}$ are pairwise different Fredholm eigenvalues of $\mathcal{O}$ and $\{\rho_k^2\}$ the corresponding residues, two geometrically similar copies $\mathcal{O}_1$ and $\mathcal{O}_2$ of $\mathcal{O}$ lead to a fatal failure for

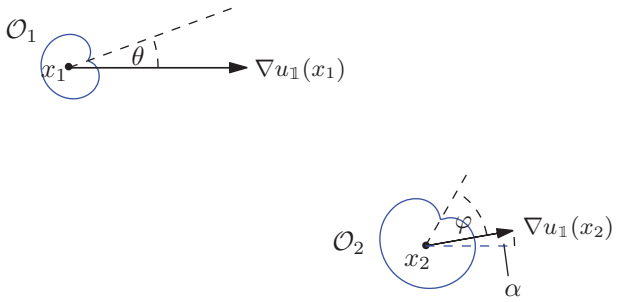

Figure 3. *Sketch of the geometrical setup of Example 8.3.*

almost any orientation of the gradients of the background potential. For obstacles with such a special shape this is a much more general counterexample than the standard fatal failure setup considered in Example 6.3. Note that polarization tensors of the form (8.10) occur, for example, when $\mathcal{O}$ is reflection symmetric with respect to one of the coordinate axes (cf. (2.10)).

Example 8.3. For a concrete example let $\mathcal{O}_1$ and $\mathcal{O}_2$ be ellipses again, with the same (nonzero) eccentricity but, possibly, different sizes $|\mathcal{O}_1| = \rho^2$ and $|\mathcal{O}_2| = \sigma^2$. Assume further that the major half axis of $\mathcal{O}_1$ forms an angle $\theta \neq j\pi/2$ to $\nabla u_{\mathbb{1}}(x_1)$, and that the major half axis of $\mathcal{O}_2$ forms an angle $\varphi \neq k\pi/2$ to $\nabla u_{\mathbb{1}}(x_2)$ (for any values of $j, k \in \mathbb{Z}$). Finally, without loss of generality, fix $\nabla u_{\mathbb{1}}(x_1) = |\nabla u_{\mathbb{1}}(x_1)|e_1$ and denote by α the angle between e_1 and $\nabla u_{\mathbb{1}}(x_2)$ (see Figure 3 for an illustration with a general reflection symmetric reference domain). Then

$$p_1(\omega) = |\nabla u_{\mathbb{1}}(x_1)|\,\rho^2 \begin{bmatrix} \dfrac{\cos^2\theta}{\lambda - \lambda_{\mathcal{E}}} + \dfrac{\sin^2\theta}{\lambda + \lambda_{\mathcal{E}}} \\ \dfrac{\sin\theta\,\cos\theta}{\lambda - \lambda_{\mathcal{E}}} - \dfrac{\sin\theta\,\cos\theta}{\lambda + \lambda_{\mathcal{E}}} \end{bmatrix}$$

with $\lambda = \lambda^{(1)}(\omega)$ and $\lambda_{\mathcal{E}}$ as in (2.9), and

$$p_2(\omega) = |\nabla u_{\mathbb{1}}(x_2)|\,\sigma^2 \begin{bmatrix} \dfrac{\cos\varphi\,\cos(\varphi+\alpha)}{\lambda - \lambda_{\mathcal{E}}} + \dfrac{\sin\varphi\,\sin(\varphi+\alpha)}{\lambda + \lambda_{\mathcal{E}}} \\ \dfrac{\cos\varphi\,\sin(\varphi+\alpha)}{\lambda - \lambda_{\mathcal{E}}} - \dfrac{\sin\varphi\,\cos(\varphi+\alpha)}{\lambda + \lambda_{\mathcal{E}}} \end{bmatrix},$$

and a straightforward computation demonstrates that

$$p_1(\omega) = \frac{|\nabla u_{\mathbb{1}}(x_1)|}{|\nabla u_{\mathbb{1}}(x_2)|}\, Y_{12} Q_\alpha^*\, p_2(\omega)\,,$$

where Y_{12} is as in (8.4), (8.5) with $c_k = \tilde{c}_k = 1$, and Q_α is as in (2.8). Since Y_{12} is nonsingular, this proves the fatal failure of the multifrequency MUSIC scheme for this example. ■

When $N_2 \neq \emptyset$ in (8.9) the shapes $\mathcal{O}_1$ and $\mathcal{O}_2$ cannot be geometrically similar. However, we don't know of any example where the specific form (8.9) with $N_2 \neq \emptyset$ materializes, and it may well be that no examples of this sort exist after all.

Table 1
The behavior of Algorithm 6.2 for two similar ellipses; angles θ and φ are as in Figure 3.

$\theta = 0$	$\varphi = 0$	fatal failure	Example 6.3
	$\varphi = \pi/2$	no failure	
	$0 < \lvert\varphi\rvert < \pi/2$	weak failure	Example 6.1
$0 < \theta < \pi/2$	$\varphi \in \{0, \pi/2\}$	weak failure	Example 6.1
	$\varphi = \pm\theta$	fatal failure	Example 6.3
	$\varphi \notin \{0, \pm\theta, \pi/2\}$	fatal failure	Example 8.3

Remark 8.4. We summarize our findings for two similar ellipses with nonzero eccentricity and identical material parameters. Define, as in Figure 3, angles $\theta \in [0, \pi/2)$ and $\varphi \in (-\pi/2, \pi/2]$ that rotate the gradients of the background potentials onto corresponding half axes of the two ellipses. Then, depending on the interplay of these two angles, Algorithm 6.2 performs as specified in Table 1 (see the links to the corresponding examples for the detailed discussion).

Accordingly, the multifrequency MUSIC scheme almost always fails for two geometrically similar ellipses with identical material parameters. ■

Remark 8.5. The case where one of the two shapes $\mathcal{O}_1$ or $\mathcal{O}_2$ fails to be simple has not yet been settled completely. However, important examples of nonsimple shapes are those that are invariant under rotations by $2\pi/k$ for integers $k \geq 3$ (cf. [9]). The corresponding polarization tensors have the form

$$M(\cdot; \mathcal{O}) = M_{11}(\cdot; \mathcal{O})\, I\,,$$

where I is the 2×2 identity matrix and, hence, if $\mathcal{O}_1$ (or $\mathcal{O}_2$) happens to be a shape of this form then Example 6.3 provides the only possible setting for a fatal failure. This we have seen at the very beginning of this section.

The performance of the multifrequency MUSIC scheme for other nonsimple domains remains an open problem. ■

9. Weak failures of the multifrequency MUSIC scheme, and how to cure them. Recall from section 6 that for two given obstacles Ω_1 and Ω_2 in $\mathcal{D}$ a weak failure of the multifrequency MUSIC scheme arises if the algorithm is capable of detecting the inclusion at $x = x_2$, but fails to locate the other one. As we have seen in section 6 (cf. (6.10)) if this situation occurs then all dipole moments $p_1(\omega_n)$ are parallel to e_1, that is, to $\nabla u_{\mathbb{1}}(x_1)$, but the dipole moments $p_2(\omega_n)$ span the whole two dimensional space (cf. also Example 6.1).

Choosing any of the frequencies ω_n, $n \in \mathbb{N}$, it follows from (3.1) that the corresponding relative data h_n^δ satisfy

$$\frac{1}{\delta^2}\, h_n^\delta \;\approx\; h_n^\circ = c_n \nabla u_{\mathbb{1}}(x_1) \cdot \nabla_z N(\cdot, x_1) + p_2(\omega_n) \cdot \nabla_z N(\cdot, x_2)$$

for some $c_n \in \mathbb{C}$ and, hence, that for $z = x_1$,

$$\phi_{z,p_z} \in \operatorname{span}\{h_n^\circ \mid n \in \mathbb{N}\} \oplus \operatorname{span}\{e_1 \cdot \nabla_z N(\cdot, x_2),\; e_2 \cdot \nabla_z N(\cdot, x_2)\}\,, \tag{9.1}$$

where ϕ_{z,p_z} is as in (3.3) with p_z of (3.4).

Moreover, as in Proposition 3.1 one can prove that the test (9.1) holds true if and only if $z \in \{x_1, x_2\}$. Using h_n^δ instead of h_n°, we can approximate the right-hand side of (9.1) to test whether $z \in \mathcal{D}$ is the (approximate) location x_1 of the other obstacle. Accordingly, weak failures are easy to cure by a simple postprocessing step without spoiling the simplicity of the basic algorithm.

10. Numerical examples. In this section we provide two numerical examples for the multifrequency MUSIC scheme. In these examples $\mathcal{D}$ is the unit disk, and the spatial component f of the AC boundary current is given by

$$f(x) = \cos\vartheta\,, \qquad x = (\cos\vartheta, \sin\vartheta) \in \partial\mathcal{D}\,,$$

so that $u_{\mathbb{1}}(x)$ is the first coordinate of the spatial variable and $\nabla u_{\mathbb{1}}(x) = e_1$ for every $x \in \mathcal{D}$. All obstacles to be considered below have the same material parameters $\sigma_l = 0.5$ and $\varepsilon_l = 1$, and data (on $\Gamma = \partial\mathcal{D}$) are generated with a boundary integral equation method for $n_* = 8$ driving frequencies

$$\begin{array}{llll} \omega_1 = 0.02, & \omega_2 = 0.1, & \omega_3 = 0.2, & \omega_4 = 0.3, \\ \omega_5 = 0.5, & \omega_6 = 1, & \omega_7 = 2, & \omega_8 = 10. \end{array}$$

Our visualizations of the numerical reconstructions show the logarithm of the cotangents of the angle between the test functions $\phi_{z,p}$ (minimized over p for Algorithm 6.2) and the span of the dominating singular functions of $A_\delta : \mathbb{R}^{n_*} \to L^2_\diamond(\Gamma)$. These numbers are large (corresponding to a hot spot of the reconstruction) when the angle is close to zero so that the test point approximates the location of a certain obstacle, while they are moderate elsewhere.

To begin with we note that for two obstacles of finite extent it is difficult to distinguish a failure of Algorithm 6.2 from its generic behavior because the rank degeneracy of $A_\circ$ is a limiting effect as $\delta \to 0$ which is somewhat blurred when $\delta > 0$. However, as soon as a third generic obstacle is present the failure of the algorithm is discernible. In that case the range of $A_\circ$ is spanned by the two independent dipoles located in the additional obstacle and by one or two combinations of dipoles located in the other two obstacles; the three or four dominating singular functions of A_δ span a subspace of $L^2_\diamond(\Gamma)$ which is a perturbation of $\mathcal{R}(A_\circ)$, while the next to leading order singular functions of A_δ have various seeds. As such, test dipoles located in the additional obstacle fit very well into the range of A_δ and this determines the amplitude of the colorbar for the function to be visualized, whereas the match of the other ones is much poorer and therefore has no observable impact on the visualization.

Accordingly we only show numerical examples with three obstacles in this section. The first of these examples treats a generic situation without failure of the algorithm, where three inclusions are located in the E, N, and SW of the disk, respectively. Figure 4 shows the corresponding reconstruction together with the exact contours of the three obstacles which are small, but far from "infinitesimal." We mention that the two obstacles in the E and SW have been generated by cubic interpolation of a few handpicked points on the boundary; the obstacle in the N is an ellipse. In this figure the left-hand plot provides the reconstruction of the traditional MUSIC scheme with the test dipole moment (3.4) proposed in [1]; the right-hand image, on the other hand, shows the result of Algorithm 6.2, minimizing for each test point $z \in \mathcal{D}$ the angle between $\phi_{z,p}$ and the span of the six dominating singular functions of

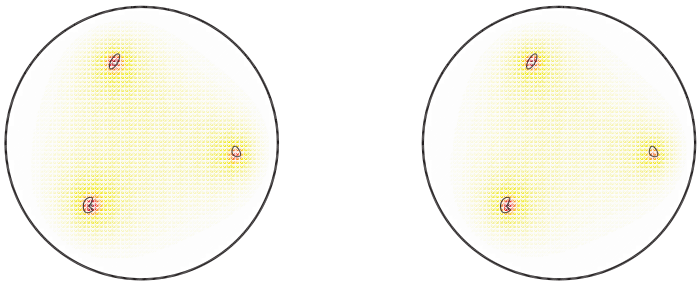

Figure 4. *Three inclusions: generic case. Traditional MUSIC scheme with p_z of (3.4) (left) and Algorithm 6.2 (right).*

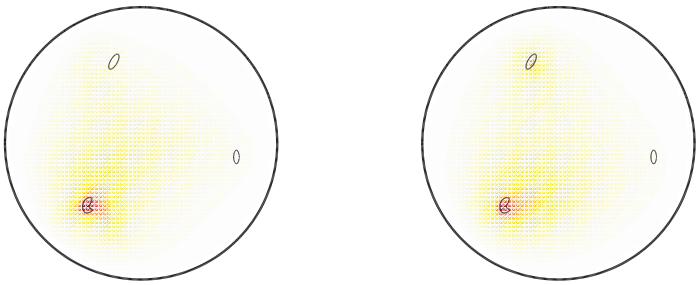

Figure 5. *Three inclusions that cause a failure. Traditional MUSIC scheme with p_z of (3.4) (left) and Algorithm 6.2 (right).*

A_δ over 32 dipole moments $p \in \mathbb{S}^1$. Note that there is no substantial difference between the two reconstructions.

For a second example we replace the obstacle in the E by another ellipse that is geometrically similar to the one in the N but is aligned with the coordinate axes, so that the two ellipses match the description in Example 6.1. Accordingly, the traditional MUSIC scheme from [1] should encounter a fatal failure for this second case, i.e., this algorithm should only detect the obstacle in the SW, given that this obstacle doesn't introduce additional problems—the generic situation. The multifrequency MUSIC scheme (Algorithm 6.2), on the other hand, should also find the ellipse in the N and only fail to find the new ellipse in the E (weak failure). As can be seen in Figure 5, this is indeed the case.

Figure 6 shows the singular values of A_δ for the two cases: The dots are the singular values for the second example (the problematic one), the circles are the ones for the generic example. In either case the singular values drop extremely rapidly—indicating the ill-posedness of the problem—but interestingly enough, the difference is not as big as one might expect. For the numerical reconstructions shown above, the test dipoles $\phi_{z,p}$ have always been projected onto the span of the left singular vectors corresponding to the $k_* = 6$ dominating singular values as indicated by the dashed line in Figure 6. However, the reconstructions don't change significantly when $k_* \in \{5, 6, 7\}$; only when the full range of A_δ is used ($k_* = 8$) are all three obstacles barely visible due to the presence of the higher order terms in A_δ.

Finally, Figure 7 demonstrates the effect of the postprocessing step outlined in section 9, once the positions of the two obstacles in the N and SW have been identified from the right-

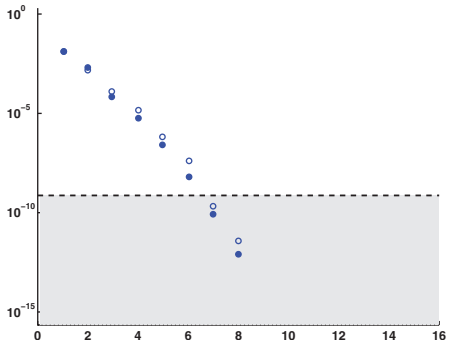

Figure 6. *Singular values for the two numerical examples.*

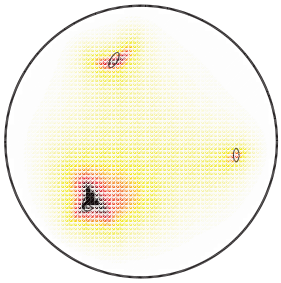

Figure 7. *Reconstruction after postprocessing, based on the right-hand plot in Figure 5.*

hand plot in Figure 5. In Figure 7 the ellipse in the E can also be detected; of course, the reconstruction of the previously determined obstacles is much brighter now (in fact, the color bar has been cropped at the old maximal value to compensate for this effect) because the associated dipoles have been appended to the range of $A_\circ$. We mention that this second run gives no improvement at all, if only the obstacle in the SW has been identified after the first run—as is the case for the original scheme with the test function (3.7).

11. Concluding remarks. We have shown that the multifrequency MUSIC scheme (Algorithm 6.2) can be used as an imaging technique to locate several small obstacles within a homogeneous conducting medium from AC current/voltage measurements on the boundary, provided that enough probing frequencies can be applied and that the gradient of the background potential is nonzero.

We have also discussed certain degenerate instances (depending on the shape of the obstacle, its material parameters, and its orientation relative to the electric current flow in the homogeneous reference medium), where the given data do not suffice to identify the material parameters and the shape of a single object; these configurations include certain ellipses, but it is not yet known whether shapes other than ellipses exist that satisfy the corresponding requirements. When the material parameters are known or can be identified, the data are rich enough to provide shape information as well (cf. [9]). It remains an open problem as to what extent the shape is uniquely determined in this case.

The multifrequency MUSIC scheme does always locate a single obstacle. In the presence of two obstacles the method may run into weak and/or fatal failures, i.e., geometric configurations

where only one or none of the obstacles can be found. A weak failure is easy to cure with a simple postprocessing step. Fatal failures, on the other hand, can only be cured with modifications that have higher computational complexity. On the other hand, the good news is that fatal failures are rare; they occur in the following cases:

(a) Both obstacles satisfy the aforementioned requirements that prevent the identification of their (different) material parameters from the given data (Theorem 7.1).
(b) The two obstacles are geometrically similar, have the same material parameters, and their orientation is aligned with the gradient of the background field (Example 6.3).
(c) Both obstacles are geometrically similar to a reference shape, the polarization tensor of which is a diagonal matrix, e.g., a shape that exhibits a reflection symmetry (Example 8.3).
(d) The two (nonsimilar) obstacles have polarization tensors of a very special form (see Theorem 8.2); yet we don't know whether there are any examples beyond those in (c) for which this is the case.

Items (b) and (c) extend to shapes that are only polarization equivalent in the sense of Definition 2.2 to the ones listed above.

This enumeration may be incomplete in that we did not fully analyze fatal failures for shapes that aren't simple in the sense of Definition 8.1. As for item (d) it can be contested whether nonsimple shapes lead to further counterexamples of any significant relevance.

REFERENCES

[1] H. Ammari, T. Boulier, and J. Garnier, *Modeling active electrolocation in weakly electric fish*, SIAM J. Imaging Sci., 6 (2013), pp. 285–321.
[2] H. Ammari and H. Kang, *Polarization and Moment Tensors with Applications to Inverse Problems and Effective Medium Theory*, Springer, New York, 2007.
[3] M. Brühl, M. Hanke, and M.S. Vogelius, *A direct impedance tomography algorithm for locating small inhomogeneities*, Numer. Math., 93 (2003), pp. 635–654.
[4] D.J. Cedio-Fengya, S. Moskow, and M.S. Vogelius, *Identification of conductivity imperfections of small diameter by boundary measurements. Continuous dependence and computational reconstruction*, Inverse Problems, 14 (1998), pp. 553–595.
[5] M. Cheney, D. Isaacson, and J.C. Newell, *Electrical impedance tomography*, SIAM Rev., 41 (1999), pp. 85–101.
[6] M. Cheney, *The linear sampling method and the MUSIC algorithm*, Inverse Problems, 17 (2001), pp. 591–595.
[7] A.J. Devaney, *Super-Resolution Processing of Multi-Static Data using Time Reversal and MUSIC*, manuscript, 2000.
[8] A.J. Devaney, *Mathematical Foundations of Imaging, Tomography and Wavefield Inversion*, Cambridge University Press, Cambridge, 2012.
[9] R. Griesmaier and M. Hanke, *Polarization Tensors of Planar Domains as Functions of the Admittivity Contrast*, preprint, arXiv:1410.4916 [math.AP] (2014).
[10] M. Hanke, *Locating several small inclusions in impedance tomography from backscatter data*, SIAM J. Numer. Anal., 49 (2011), pp. 1991–2016.
[11] V. Isakov, *Inverse Problems for Partial Differential Equations*, 2nd ed., Springer, New York, 2006.
[12] D. Khavinson, M. Putinar, and H.S. Shapiro, *Poincaré's variational problem in potential theory*, Arch. Ration. Mech. Anal., 185 (2007), pp. 143–184.
[13] A. Kirsch, *The MUSIC algorithm and the factorization method in inverse scattering theory for inhomogeneous media*, Inverse Problems, 18 (2002), pp. 1025–1040.
[14] R. Kress, *Linear Integral Equations*, 3rd ed., Springer, New York, 2014.

[15] J. Plemelj, *Potentialtheoretische Untersuchungen*, B.G. Teubner, Leipzig, 1911.
[16] B. Scholz, *Towards virtual electrical breast biopsy: Space frequency MUSIC for trans-admittance data*, IEEE Trans. Med. Imaging, 21 (2002), pp. 588–595.
[17] B. Scholz and R. Anderson, *On electrical impedance scanning—principles and simulations*, Electromedica, 68 (2000), pp. 35–44.
[18] C.W. Therrien, *Discrete Random Signals and Statistical Signal Processing*, Prentice-Hall, Englewood Cliffs, NJ, 1992.